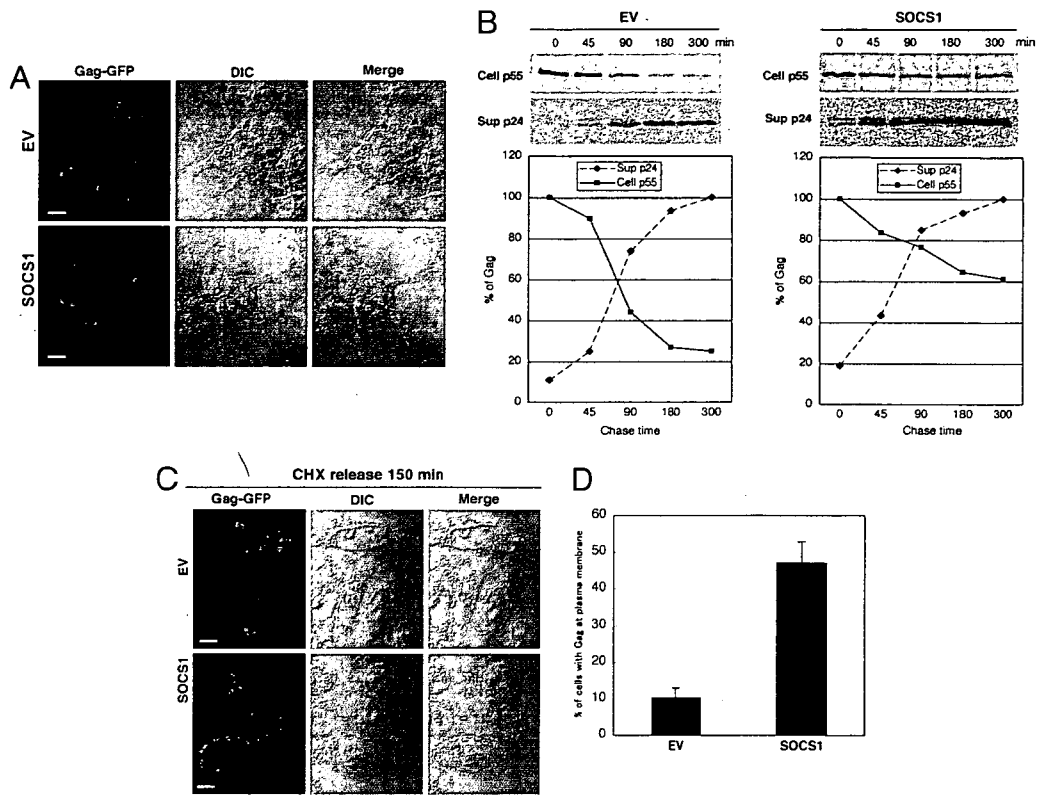

Fig. 3. SOCS1 enhances both the stability and trafficking of HIV-1 Gag. (*A*) HeLa cells cotransfected with pNL4-3 and either control vector (EV) or SOCS1 were immunostained with antibodies targeting anti-p24 (CA). Confocal microscopy with differential interference contrast (DIC) was then performed. (Scale bars: 10 μm.) (*B*) 293T cells were transfected with either a control empty vector (EV) (*Left*) or myc-SOCS1 (*Right*) and cotransfected with pNL4-3. After 48 h, cells were pulse-labeled with [^{35}S]methionine or [^{35}S]cysteine for 15 min and chased for the durations indicated. Cell lysates and pelleted supernatant virions were immunoprecipitated with anti-p24 antibodies followed by autoradiography. (*C* and *D*) HeLa cells seeded on poly-L-lysine-coated cover slides were transfected with either vector control or SOCS1. After 24 h, cells were again transfected with Gag-GFP for 3 h and then treated with 100 μg/ml CHX for 5 h to inhibit protein synthesis. This treatment was followed by incubation with fresh medium; then 150 min after the CHX release, cells were fixed and subjected to confocal microscopy (*C*). (Scale bars: 10 μm.) Cells with Gag protein on the plasma membrane were scored out of 200 transfected cells (*D*).

p55 Gag, whereas an N-terminal or a SOCS box deletion did not affect the binding of SOCS1 to Gag in 293T cells (Fig. 2*E*). This finding indicates that the SH2 domain is important for the interaction of SOCS1 with HIV-1 Gag. Interestingly, the R105E mutant of SOCS1, which disrupts the function of the SH2 domain, still binds Gag (Fig. 2*E*), indicating that the Gag–SOCS1 association is independent of the tyrosine phosphorylation of Gag, as is the case for both HPV-E7 and Vav (16, 17).

To elucidate the SOCS1-binding region of the Gag protein, GST pull-downs with various GST-fused Gag domain constructs were performed. SOCS1 was detected in glutathione bead precipitates with GST-wild-type Gag, GST-Δp6, GST-MA, and GST-NC, but not with other domain constructs (Fig. 2*F*), indicating that SOCS1 interacts with Gag via its MA and NC domains. Consistent with these results, the deletion of both the MA and NC domains of p55 Gag (ΔMAΔNC) completely abolishes its interaction with SOCS1 in coimmunoprecipitation experiments (Fig. 2*G*). Furthermore, *in vitro* analysis with purified proteins also demonstrated that SOCS1 can indeed interact with both the MA and NC regions of HIV-1 Gag in the absence of nucleic acids or other proteins (SI Fig. 5).

We next wished to determine the functional interaction domain in HIV-1 Gag through which SOCS1 functions in terms of virus-like particle production. To this end, we used a MA-deleted Gag mutant with an N-terminal myristoyl tag derived from src (ΔMA-src) (18) and also an NC-deleted Gag mutant with a GCN4 leucine zipper in place of NC, which we herein denote as ΔNC-LZ but which has been described as Z_{IL}-p6 (19). Both of these mutants have been shown still to assemble and bud (18, 19). We found that SOCS1 overexpression can still augment the particle formation of both wild-type Gag and ΔNC-LZ but not ΔMA-src (Fig. 2*H*), indicating that the functional interaction between SOCS1 and HIV-1 Gag is in fact mediated through MA.

To confirm further the direct interaction between SOCS1 and Gag in cells, we examined the intracellular localization of these two proteins. Confocal microscopy revealed that endogenous SOCS1 forms dotted filamentous structures in the cytoplasm and that Gag localizes in a very punctate pattern with SOCS1 from the perinuclear regions to the cell periphery (Fig. 2*I*). These data indicate that SOCS1 interacts with HIV-1 Gag in the cytoplasm during HIV-1 particle production.

SOCS1 Promotes both the Stability of Gag and Its Targeting to the Plasma Membrane. Because we had found from our initial data that SOCS1 increases HIV-1 particle production as a result of its direct interaction with intracellular Gag proteins, we next addressed whether SOCS1 positively regulates Gag stability and subsequent trafficking to PM. Our immunofluorescent analysis with the anti-p24 (CA) antibody initially revealed that SOCS1 overexpression increases the levels of Gag at PM when cotransfected with pNL4-3 at 48 h after transfection, although it was detected at PM in both control and SOCS1-expressing cells (Fig. 3*A*). Furthermore, the levels of cytoplasmic Gag were found to be much lower in the SOCS1-expressing cells compared with the control cells (Fig. 3*A*). These results indicate that SOCS1 enhances Gag trafficking to PM.

To examine next whether SOCS1 affects the stability and trafficking of newly synthesized Gag proteins, we performed pulse–chase analysis. This experiment revealed that SOCS1 significantly increases the stability of the intracellular p55 Gag polyprotein as well as the levels of p24 in the supernatant (Fig. 3*B*). Importantly, p24 was detectable at an earlier time point and reached maximum levels in a shorter period in the cell supernatant of SOCS1-transfected cells compared with control vector-transfected cells (Fig. 3*B*). This finding again suggests that SOCS1 facilitates the intracellular trafficking of newly synthesized Gag proteins to PM.

To confirm this hypothesis further, we performed cycloheximide (CHX) analysis with HeLa cells transfected using either vector control or SOCS1. After 24 h, cells were again transfected with Gag-GFP for 3 h and treated with CHX for 5 h to inhibit protein synthesis. Cells were then cultured in fresh medium without CHX for an additional 150 min and subjected to confocal microscopy. At

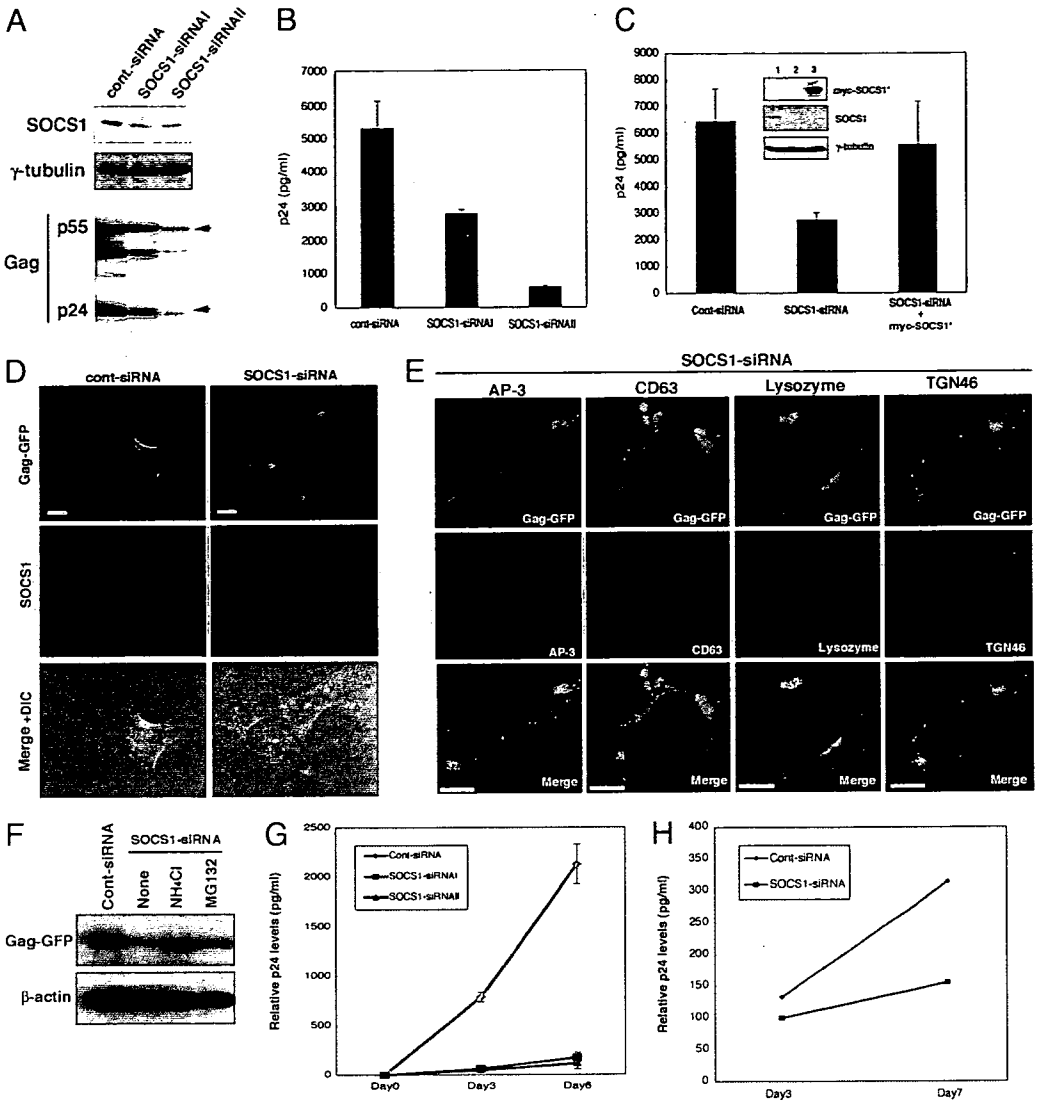

Fig. 4. The targeted inhibition of SOCS1 suppresses Gag trafficking and HIV-1 particle production and enhances Gag degradation in lysosomes. (*A* and *B*) 293T cells were transfected with either control siRNA or two different SOCS1-specific siRNAs (I or II) together with pNL4-3. At 48 h after transfection, cell lysates were subjected to immunoblotting analysis with the indicated antibodies (*A*). Cell supernatants were then subjected to ELISA analysis of p24 levels (*B*). (*C*) 293T cells were transfected with pNL4-3 and cotransfected with control-siRNA, SOCS1-siRNAI alone, or SOCS1-siRNAI plus siRNA-resistant myc-SOCS1 (myc-SOCS1*). After 48 h, cell supernatants were collected and subjected to p24 ELISA. (*Inset*) Immunoblots of the cell lysates. (*D*) HeLa cells were transfected with control or SOCS1-specific siRNA and cotransfected with GFP-Gag. At 48 h after transfection, the cells were subjected to confocal microscopy. (*E*) HeLa cells were transfected with Gag-GFP and SOCS1-siRNA constructs for 48 h. Cells were then fixed and subjected to immunofluorescent analysis with indicated antibodies followed by DAPI staining. (Scale bars: 10 mm.) (*F*) HeLa cells were transfected with Gag-GFP and cotransfected with either control-siRNA or SOCS1-siRNA. After 36 h, the cells were treated with a mock solution, 10 mM NH_4Cl or 10 μM MG132 for another 16 h. Cell were then harvested and subjected to immunoblotting analysis with anti-GFP or anti-β-actin antibodies. (*G*) Jurkat cells were infected with a retroviral vector encoding control (Cont) or two different SOCS1-specific siRNAs (I or II). After selection with puromycin, the cells were then infected with HIV-1_{NL4-3} (multiplicity of infection, 0.1), and p24 antigen levels in cell supernatant were measured by ELISA at the indicated time points. (*H*) Human primary CD4 T cells were separated from healthy donors and infected with lentivirus vectors encoding either control- or SOCS1-siRNAI. The cells were then infected with HIV-1_{NL4-3} (multiplicity of infection, 0.1), and p24 antigen levels in cell supernatant were measured by ELISA at the indicated time points.

this time point, Gag-GFP was found to localize predominantly in a perinuclear region in the control cells (Fig. 3*C*), whereas almost half of the SOCS1-transfected cells exhibited Gag-GFP localization on PM (Fig. 3*D*). These results again indicate that SOCS1 efficiently enhances the trafficking of newly synthesized Gag protein to PM.

The Targeted Disruption of SOCS1 Inhibits Gag Trafficking and HIV-1 Particle Production. To delineate further the role of SOCS1 in the trafficking of Gag and in subsequent HIV-1 particle production, we depleted cellular SOCS1 by siRNA. The significant depletion of SOCS1 expression by two different SOCS1-specific siRNA constructs was confirmed by immunoblotting analysis (Fig. 4 *A* and *B*). Significantly, in cells cotransfected with pNL4-3 and SOCS1-specific siRNAs, both HIV-1 particle release and the levels of intracellular Gag protein are significantly decreased compared with the control cells (Fig. 4 *A* and *B*). Furthermore, the effects of SOCS1-siRNA on the inhibition of HIV-1 particle production was diminished by reexpression with a codon-optimized SOCS1 construct that is resistant to these siRNAs (Fig. 4*C*), indicating that the SOCS1 siRNA suppression of HIV-1 particle production depends on the availability of endogenous SOCS1.

Consistent with these observations, immunofluorescent analysis further revealed that the expression of SOCS1-siRNA dramatically inhibits Gag trafficking such that Gag proteins accumulate in the perinuclear regions as large solid aggregates, as has been reported (20) (Fig. 4*D*). This finding indicates that SOCS1 plays an essential role in the Gag trafficking from perinuclear clusters to PM. Interestingly, these discrete perinuclear clusters of Gag were found to colocalize with lysosome markers, lysozyme, and partly with AP-3, but neither with the late endosome MVB marker CD63 nor the *trans*-Golgi marker TGN46, indicating that Gag is targeted for degradation by lysosomes when the function of SOCS1 is inhibited (Fig. 4*E*). In support of this notion, the levels of intracellular Gag were found to be significantly increased by treatment with a lysosome inhibitor NH_4Cl but not by a proteasome inhibitor MG132 in SOCS1-siRNA cells (Fig. 4*F*), further indicating that the perinuclear clusters of Gag will undergo lysosomal degradation rather than proteasomal degradation when optimal Gag transport to PM is suppressed by the inhibition of SOCS1.

We next addressed whether targeted SOCS1 inhibition would affect HIV-1 particle production in human T cells. The effect of SOCS1 depletion was clearly evident in both HIV-1_{NL4-3}-infected

Jurkat cells and human primary $CD4^+$ T cells, which demonstrated pronounced decreases in virus particle production in SOCS1-siRNA-expressed cells compared with the controls (Fig. 4 *G* and *H*). These results together indicate that the specific inhibition of SOCS1 suppresses the optimal trafficking of Gag to PM, resulting in the degradation of Gag in lysosomes, which in turn leads to the efficient and reproducible inhibition of HIV-1 particle production in various types of human cells.

Discussion

In this work, we report that SOCS1 is an inducible host factor during HIV-1 infection and plays a key role in the late stages of the viral replication pathway via an IFN-independent mechanism (SI Fig. 6). These results represent evidence that SOCS1 is a potent host factor that facilitates HIV-1 particle production via posttranscriptional mechanisms.

SOCS1 has been shown to be a suppressor of several cytokine signaling pathways, and like all SOCS family members it has a central SH2 domain and a conserved C-terminal domain known as the SOCS box (21, 22). Structure–function analyses have further demonstrated that the SOCS1 SH2 domain is required for the efficient binding of its substrates (23, 24). Indeed, our current analyses have also revealed that the SH2 domain of SOCS1 is required for its interaction with the HIV-1 Gag protein. We have shown from our present data that the SOCS box is also required for SOCS1 to function during HIV-1 particle production.

The SOCS box-mediated function of SOCS1 is chiefly exerted via its ubiquitin ligase activity (21, 25). Biochemical binding studies have shown that the SOCS box of SOCS1 interacts with the elongin BC complex, a component of the ubiquitin/proteasome pathway that forms an E3 ligase with Cul2 (or Cul5) and Rbx-1 (21, 26, 27). We show from our current experiments that the SOCS box is required for HIV-1 particle production, indicating the involvement of the ubiquitin/proteasome pathway. However, it is still unknown whether SOCS1 promotes the ubiquitination of Gag and, if so, whether the mono- or poly-ubiquitination of Gag would affect its trafficking and protein stability. Further studies will be necessary to clarify the biological significance of Gag ubiquitination.

Perlman and Resh (20) recently reported that newly synthesized Gag first appears to be diffusely distributed in the cytoplasm, accumulates in perinuclear clusters, passes transiently through a MVB-like compartment, and then traffics to PM. Consistent with these observations, our current work also shows that Gag is accumulated at perinuclear clusters as solid aggregates when its targeting to PM is impaired because of the SOCS1 inhibition.

Another aspect of SOCS1 function during HIV-1 infection was proposed recently. Song *et al.* (28) reported that SOCS1-silenced dendritic cells broadly induce the enhancement of HIV-1 Env-specific $CD8^+$ cytotoxic T lymphocytes and $CD4^+$ T helper cells as well as an antibody response. The induction of the SOCS1 gene in HIV-1 infected cells might therefore disrupt a specific intracellular immune response to HIV-1 in infected host cells.

Based on the strong evidence that we present in our current work that SOCS1 positively regulates the late stages of HIV replication, we conclude that SOCS1 is likely to be a valuable therapeutic target not only for future treatments of AIDS and related diseases, but also for a postexposure prophylaxis against disease in HIV-1-infected individuals.

Materials and Methods

Antibodies and Fluorescent Reagents. Antibodies and fluorescent reagents were obtained from the following sources. Anti-CD63, anti-AP-3, anti-myc (A-14), and anti-SOCS1 (H-93) were from Santa Cruz Biotechnology. Anti-SOCS1 was from Zymed Laboratories. Anti-FLAG (M2) and anti-HA (12CA5) were from Sigma and Roche Diagnostics, respectively. Anti-HIV-p24 (Dako; Cytomation), anti-STAT1, and anti-phospho-STAT1 (Y701) were from BD Transduction Laboratories. Sheep polyclonal anti-TGN46 was from GeneTex.

Plasmid Constructs. Expression constructs for SOCS1 have been described in ref. 29. GST fusion constructs with specific regions derived from the codon-optimized *gag* were generated (MA, CA, NC, p6, Δp6, full-length Gag) by cloning into pGEX-2T (GE Healthcare Bio-Sciences) as described in ref. 30. For retrovirus-mediated siRNA expression, pSUPER.retro.puro vector was digested, as described in ref. 31, with the following sequences: SOCS1-siRNAI, TCGAGCTGCTGGAGCACTA; SOCS1-siRNAII, GGCCAGAACCTTCCTCCTCTT; control siRNA, TCGTATGTTGTGTGGAATT.

Electron Microscopy. Transfected 293T cells were fixed with 2.5% glutaraldehyde and subjected to TEM, as described (14, 32).

ACKNOWLEDGMENTS. We thank Dr. H Gottlinger (University of Massachusetts) for providing plasmids. This work was supported in part by grants from the Ministry of Education, Culture, Sports, Science, and Technology of Japan and Human Health Science of Japan.

1. Sorin M, Kalpana GV (2006) *Curr HIV Res* 4:117–130.
2. Freed EO (2004) *Trends Microbiol* 12:170–177.
3. Peterlin BM, Trono D (2003) *Nat Rev Immunol* 3:97–107.
4. Trkola A (2004) *Curr Opin Microbiol* 7:555–559.
5. Freed EO (1998) *Virology* 251:1–15.
6. Adamson CS, Jones IM (2004) *Rev Med Virol* 14:107–121.
7. VerPlank L, Bouamr F, LaGrassa TJ, Agresta B, Kikonyogo A, Leis J, Carter CA (2001) *Proc Natl Acad Sci USA* 98:7724–7729.
8. Garrus JE, von Schwedler UK, Pornillos OW, Morham SG, Zavitz KH, Wang HE, Wettstein DA, Stray KM, Cote M, Rich RL, *et al.* (2001) *Cell* 107:55–65.
9. Strack B, Calistri A, Craig S, Popova E, Gottlinger HG (2003) *Cell* 114:689–699.
10. Dong X, Li H, Derdowski A, Ding L, Burnett A, Chen X, Peters TR, Dermody TS, Woodruff E, Wang JJ, *et al.* (2005) *Cell* 120:663–674.
11. Alroy I, Tuvia S, Greener T, Gordon D, Barr HM, Taglicht D, Mandil-Levin R, Ben-Avraham D, Konforty D, Nir A, *et al.* (2005) *Proc Natl Acad Sci USA* 102:1478–1483.
12. Ryo A, Suzuki Y, Ichiyama K, Wakatsuki T, Kondoh N, Hada A, Yamamoto M, Yamamoto N (1999) *FEBS Lett* 462:182–186.
13. Adachi A, Gendelman HE, Koenig S, Folks T, Willey R, Rabson A, Martin MA (1986) *J Virol* 59:284–291.
14. Demirov DG, Ono A, Orenstein JM, Freed EO (2002) *Proc Natl Acad Sci USA* 99:955–960.
15. Chang TL, Mosoian A, Pine R, Klotman ME, Moore JP (2002) *J Virol* 76:569–581.
16. De Sepulveda P, Okkenhaug K, Rose JL, Hawley RG, Dubreuil P, Rottapel R (1999) *EMBO J* 18:904–915.
17. Kamio M, Yoshida T, Ogata H, Douchi T, Nagata Y, Inoue M, Hasegawa M, Yonemitsu Y, Yoshimura A (2004) *Oncogene* 23:3107–3115.
18. Gallina A, Mantoan G, Rindi G, Milanesi G (1994) *Biochem Biophys Res Commun* 204:1031–1038.
19. Accola MA, Strack B, Gottlinger HG (2000) *J Virol* 74:5395–5402.
20. Perlman M, Resh MD (2006) *Traffic* 7:731–745.
21. Alexander WS (2002) *Nat Rev Immunol* 2:410–416.
22. Marine JC, Topham DJ, McKay C, Wang D, Parganas E, Stravopodis D, Yoshimura A, Ihle JN (1999) *Cell* 98:609–616.
23. Narazaki M, Fujimoto M, Matsumoto T, Morita Y, Saito H, Kajita T, Yoshizaki K, Naka T, Kishimoto T (1998) *Proc Natl Acad Sci USA* 95:13130–13134.
24. Yasukawa H, Misawa H, Sakamoto H, Masuhara M, Sasaki A, Wakioka T, Ohtsuka S, Imaizumi T, Matsuda T, Ihle JN, *et al.* (1999) *EMBO J* 18:1309–1320.
25. Tyers M, Rottapel R (1999) *Proc Natl Acad Sci USA* 96:12230–12232.
26. Kamizono S, Hanada T, Yasukawa H, Minoguchi S, Kato R, Minoguchi M, Hattori K, Hatakeyama S, Yada M, Morita S, *et al.* (2001) *J Biol Chem* 276:12530–12538.
27. Kamura T, Burian D, Yan Q, Schmidt SL, Lane WS, Querido E, Branton PE, Shilatifard A, Conaway RC, Conaway JW (2001) *J Biol Chem* 276:29748–29753.
28. Song XT, Evel-Kabler K, Rollins L, Aldrich M, Gao F, Huang XF, Chen SY (2006) *PLoS Med* 3:e11.
29. Ryo A, Suizu F, Yoshida Y, Perrem K, Liou YC, Wulf G, Rottapel R, Yamaoka S, Lu KP (2003) *Mol Cell* 12:1413–1426.
30. Morikawa Y, Kishi T, Zhang WH, Nermut MV, Hockley DJ, Jones IM (1995) *J Virol* 69:4519–4523.
31. Ryo A, Uemura H, Ishiguro H, Saitoh T, Yamaguchi A, Perrem K, Kubota Y, Lu KP, Aoki I (2005) *Clin Cancer Res* 11:7523–7531.
32. Nagashima Y, Nishihira H, Miyagi Y, Tanaka Y, Sasaki Y, Nishi T, Imaizumi K, Aoki I, Misugi K (1996) *Cancer* 77:799–804.

JOURNAL OF VIROLOGY, Dec. 2007, p. 13259–13264 Vol. 81, No. 23
0022-538X/07/$08.00+0 doi:10.1128/JVI.01353-07

Humanized NOD/SCID/IL2Rγ^{null} Mice Transplanted with Hematopoietic Stem Cells under Nonmyeloablative Conditions Show Prolonged Life Spans and Allow Detailed Analysis of Human Immunodeficiency Virus Type 1 Pathogenesis$^{\nabla}$

Satoru Watanabe,[1,2] Shinrai Ohta,[3] Misako Yajima,[4] Kazuo Terashima,[5] Mamoru Ito,[6] Hideo Mugishima,[7] Shigeyoshi Fujiwara,[4] Kazufumi Shimizu,[2] Mitsuo Honda,[3] Norio Shimizu,[1]* and Naoki Yamamoto[3,5]*

Department of Virology, Division of Medical Science, Medical Research Institute, Tokyo Medical and Dental University, 1-5-45 Yushima, Bunkyo-ku, Tokyo 113-8519, Japan[1]; Open Research Center for Genome and Infectious Disease Control, Nihon University School of Medicine, 30-1 Oyaguchikami-chou, Itabashi-ku, Tokyo 173-8610, Japan[2]; AIDS Research Center, National Institute of Infectious Diseases, 1-23-1 Toyama, Shinjuku-ku, Tokyo 162-8640, Japan[3]; Department of Infectious Diseases, National Research Institute for Child Health and Development, 2-10-1 Okura, Setagaya-ku, Tokyo 154-8567, Japan[4]; Department of Molecular Virology, Graduate School of Medicine, Tokyo Medical and Dental University, 1-5-45 Yushima, Bunkyo-ku, Tokyo 113-8519, Japan[5]; Central Institute for Experimental Animals, 1430 Nogawa, Miyamae-ku, Kawasaki, Kanagawa 216-0001, Japan[6]; and Department of Pediatrics and Child Health, Nihon University School of Medicine, 30-1 Oyaguchikami-chou, Itabashi-ku, Tokyo 173-8610, Japan[7]

Received 21 June 2007/Accepted 3 September 2007

In a previous study, we demonstrated that humanized NOD/SCID/IL2Rγ^{null} (hNOG) mice constructed with human hematopoietic stem cells (HSCs) allow efficient human immunodeficiency virus type 1 (HIV-1) infection. However, HIV-1 infection could be monitored for only 43 days in the animals due to their short life spans. By transplanting HSCs without any myeloablation methods, the mice successfully survived longer than 300 days with stable engraftment of human cells. The mice showed high viremia state for more than the 3 months examined, with systemic HIV-1 infection and gradual decrease of CD4$^+$ T cells analogous to that in humans. These capacities of the hNOG mice are very attractive for modeling mechanisms of AIDS progression and therapeutic strategy.

One of the main problems in the field of human immunodeficiency virus type 1 (HIV-1) research is the lack of suitable small animal models for studying the virological and pathogenic aspects of human HIV-1 infection. To overcome the drawback that HIV-1 does not replicate in rodent cells, severe combined immunodeficiency (SCID) mice, engrafted with human peripheral blood mononuclear cells (hu-PBL-SCID) (16) or human fetal thymus and liver tissue [SCID-hu (Thy/Liv)] (18), have been used for the small animal models of HIV-1 infection. However, these mouse models fall short of accurately mirroring human HIV infection because of their short infection spans (17), limited infection of lymphoid tissues (15), and partial infection to coreceptor tropic HIVs (4, 10, 13).

Considering the significant advantages of developing a mouse model for HIV-1 infection, we previously introduced a novel HIV-1 mouse model using nonobese diabetic (NOD)/SCID/interleukin-2 receptor (IL-2R) gamma chain-knocked-out (NOG) mice (22). Multilineage human cells, including T, B, NK cells, monocytes/macrophages, and dendritic cells (DCs) differentiate in the mice when transplanted with human CD34$^+$ hematopoietic stem cells (HSCs) (6, 9, 22). These mice show high levels of susceptibility to both CCR5 (R5)- and CXCR4 (X4)-tropic HIVs with intense plasma viral loads lasting for over 40 days (22). Thus, this mouse model may be valuable for the study of HIV-1 infection. However, a serious problem remains. The mice showed symptoms of a wasting condition and a hunched back 5 to 7 months after HSC transplantation, following which most of them died. This life span is not sufficient if we are to better understand HIV pathogenesis and to develop novel anti-HIV countermeasures, because more than 4 months posttransplantation is required for the development of human T cells before HIV-1 can be studied in mice.

In past studies for the construction of humanized mouse models using NOD/SCID, β2 microglobulin-deficient NOD/SCID (NOD/SCID/B2m^{null}) or NOG mice, the mice were subjected to total body irradiation or given drugs for HSC transplantation (6, 9, 11, 14, 21, 23). Since NOG mice do not develop any thymic lymphomas in contrast to NOD/SCID or NOD/SCID/B2m^{null} mice (3, 19), the irradiation might influence the reduction of their life spans. In this study, we therefore searched for optimal conditions for HSC transplantation and consequently found that in NOG mice, myeloablation procedures were not required for human cell generation. Importantly, these mice stably survived

* Corresponding author. Mailing address for Naoki Yamamoto: AIDS Research Center, National Institute of Infectious Diseases, 1-23-1 Toyama, Shinjuku-ku, Tokyo 162-8640, Japan. Phone: 81-3-5285-1111. Fax: 81-3-5285-1165. E-mail: nyama@nih.go.jp. Mailing address for Norio Shimizu: Department of Virology, Division of Medical Science, Medical Research Institute, Tokyo Medical and Dental University, 1-5-45 Yushima, Bunkyo-ku, Tokyo 113-8519, Japan. Phone and fax: 81-3-5803-5811. E-mail: nshivir@tmd.ac.jp.

$^{\nabla}$ Published ahead of print on 19 September 2007.

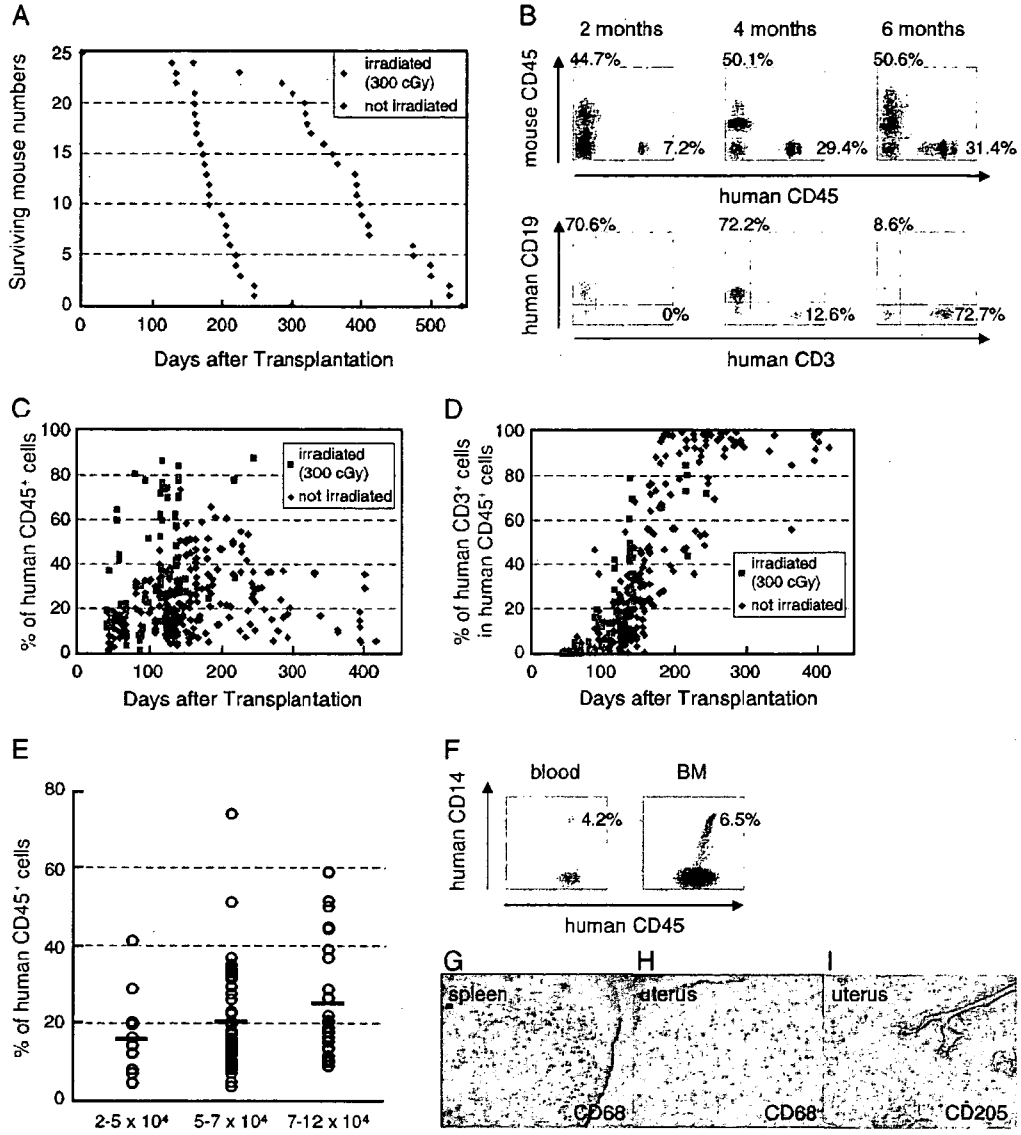

FIG. 1. Human cell generation in hematopoietic stem cell-engrafted hNOG mice with or without myeloablation. (A) Life spans of NOG mice transplanted with human stem cells after receiving 300 cGy irradiation (n = 25) or not receiving irradiation (n = 25). (B) Representative flow cytometric profiles of the mice from 2 to 6 months after transplantation without irradiation. The ratio of human to murine CD45$^+$ cells and that of human CD3$^+$ cells to CD19$^+$ cells are shown. Note that the mice generated human CD45$^+$ leukocytes that eventually developed human CD19$^+$ B cells first and then CD3$^+$ T cells. (C and D) Percentages of human CD45$^+$ cells (C) and CD3$^+$ T cells in human CD45$^+$ cells (D) in peripheral blood from 65 mice that received 300 cGy irradiation and 222 nonirradiated mice 40 to 413 days after transplantation. (E) Summary of engraftment levels in nonirradiated mice transplanted with 2×10^4 to 5×10^4 cells (n = 11), 5×10^4 to 7×10^4 cells (n = 53), or 7×10^4 to 12×10^4 (n = 30) human stem cells. Percentages of human CD45$^+$ leukocytes in peripheral blood during 4 to 5 months after transplantation were shown. The horizontal black bars indicate the averages of the groups. (F to I) Flow cytometric analysis and immunohistochemical analysis of the expression of myelomonocytic markers in nonirradiated mice 4 months after transplantation. Human CD14$^+$ monocytes/macrophages were recognized in peripheral blood and BM (F). A gate was set on the human CD45$^+$ population. Human CD68$^+$ macrophages and CD205$^+$ DCs were also detected in spleen (G) and uterus (H and I). Visualization was performed with 5-bromo-4-chloro-3-indolylphosphate (BCIP). The original magnifications were ×100 (G and H) and ×200 (I).

longer than 300 days after the HSC transplantation, which allowed further investigation of HIV-1 pathogenesis and progression to disease state in the animals.

NOG mice constructed with HSCs without myeloablation showed prolonged survival time and stable human cell generation. Six- to eight-week-old female NOG mice were obtained from the Central Institute for Experimental Animals (Kawasaki, Japan), and human cord blood-derived CD34$^+$ HSCs (2×10^4 to 12×10^4 cells) were injected intravenously with or without irradiation. As shown in Fig. 1A, most of the mice that received 300 cGy irradiation were dead within 250 days post-transplantation (mean survival time, 188 days). In contrast, more than 80% of the mice with transplanted HSCs without irradiation survived over 300 days (mean survival time, 387

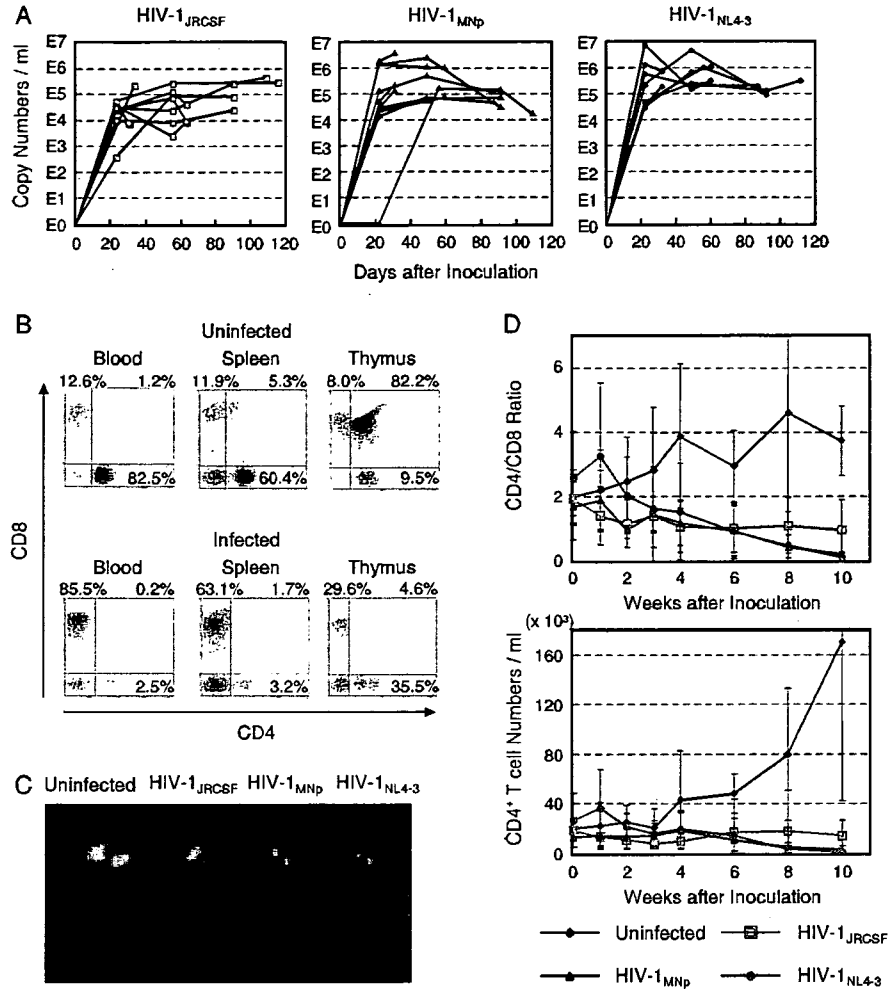

FIG. 2. Long-lasting viremia and $CD4^+$ T-cell depletion in R5- and X4-tropic HIV-1-infected hNOG mice. (A) Viral copy numbers in plasma from 29 mice intravenously inoculated with R5-tropic HIV-1_{JRCSF} (65,000 $TCID_{50}$; $n = 11$), X4-tropic HIV-1_{MNp} (20,000 $TCID_{50}$; $n = 10$), and X4-tropic HIV-1_{NL4-3} (60,000 $TCID_{50}$; $n = 8$). RNA viral copy numbers were measured using a real-time PCR quantification assay as previously described (22). (B) The percentages of $CD4^-$ $CD8^+$ (top left), $CD4^+$ $CD8^+$ (top right), and $CD4^+$ $CD8^-$ (bottom right) cells in blood, spleen, and thymus from a uninfected control mouse and a V-1_{NL4-3}-infected mouse (32 days postinfection). These two mice were constructed with HSCs from the same cord blood donor, and sacrificed 181 and 169 days after transplantation, respectively. A gate was set on the human $CD45^+$ population. (C) Comparison of the apparent size of mesenteric LN from uninfected mice or mice infected with HIV-1_{JRCSF} (109 days postinfection), HIV-1_{MNp} (109 days postinfection), or HIV-1_{NL4-3} (112 days postinfection). A uninfected control mouse was sacrificed 249 days after transplantation, and three HIV-1-infected mice were sacrificed 246, 246, and 249 days after transplantation. (D) Comparison of CD4/CD8 T-cell ratios and absolute $CD4^+$ T-cell numbers in peripheral blood from uninfected control mice ($n = 7$), R5-tropic HIV-1_{JRCSF}-infected mice ($n = 7$), X4-tropic HIV-1_{MNp}-infected mice ($n = 5$), and X4-tropic HIV-1_{NL4-3}-infected mice ($n = 6$). Results are expressed as means ± standard deviations (error bars).

days). These mice were successfully engrafted with HSCs, resulting first in the generation of human $CD19^+$ B cells and subsequently in the generation of human $CD3^+$ T cells (Fig. 1B). Figure 1C and D show the percentages of human $CD45^+$ leukocytes and human $CD3^+$ T cells in peripheral blood at 40 to 413 days after HSC transplantation. Up to 74% of leukocytes in peripheral blood samples were reconstituted with human cells in nonirradiated mice (mean ± standard deviation, 22.8% ± 14.0%; $n = 222$), and this was maintained over 400 days after transplantation (Fig. 1C). Although higher levels of human cell reconstitution were observed in the irradiated mice (45.2% ± 23.9%; $n = 65$) (Fig. 1C), which may be due to reduction of absolute numbers of murine cells by destruction of their progenitor cells in bone marrow (BM), human $CD3^+$ T cells developed with similar kinetics between the two groups (Fig. 1D). Figure 1E shows the engraftment efficiency of NOG mice transplanted with different numbers of HSCs without irradiation. More than 2×10^4 HSCs could be stably engrafted, and the levels of human cell reconstitution increased relative to the number of transplanted cells.

We further analyzed the development of human monocytes, macrophages, and DCs in the mice with transplanted HSCs without irradiation. Human $CD14^+$ monocytes were detected in peripheral blood and BM using flow cytometry (Fig. 1F), and many human $CD68^+$ macrophages were observed in various organs, including spleen (Fig. 1G), uterus (Fig. 1H), ovary, and lung (data not shown). Human $CD205^+$ DCs were also detected in spleen (data not shown) and uterus (Fig. 1I). These

TABLE 1. CD4/CD8 ratios in peripheral blood and spleen and $CD4^+$ $CD8^+$ cells in thymus of groups of uninfected and HIV-1-infected mice[a]

Group and mouse identification no.	No. of days after inoculation	CD4/CD8 ratio		% of $CD4^+$ $CD8^+$ cells in thymus	No. of RNA viral copies/ml
		Blood	Spleen		
Uninfected control group (n = 15)		2.92 ± 1.68	2.78 ± 1.46	67.8 ± 20.5	
$HIV\text{-}1_{JRCSF}$-infected group					
1	30	1.86	0.88	77.1	9,078
2	30	0.46	0.53	12.5	7,703
3	33	2.61	2.17	85.7	223,020
4	63	0.17	0.27	25.5	9,965
5	63	0.36	0.44	27.2	8,734
6	63	0.18	0.88	69.6	42,198
7	90	0.03	0.37	82.5	24,441
8	90	0.30	0.79	84.6	24,454
9	90	1.77	1.55	56.9	80,636
10	109	0.20	0.17	43.4	470,392
11	116	0.09	0.78	11.8	299,080
$HIV\text{-}1_{MNp}$-infected group					
1	31	0.82	0.44	34.6	3,709,520
2	31	1.02	0.61	90.2	219,971
3	31	1.64	1.57	78.2	135,592
4	59	0.21	0.38	35.4	78,848
5	59	0.10	0.07	77.0	1,039,716
6	87	0.20	0.40	0.5	49,080
7	87	0.19	0.08	11.7	121,817
8	91	0.04	0.04	82.9	30,706
9	91	0.28	0.10	1.2	7,407
10	109	0.00	0.21	2.8	17,310
$HIV\text{-}1_{NL4\text{-}3}$-infected group					
1	32	1.01	0.81	64.5	195,375
2	32	0.03	0.05	4.6	770,721
3	60	0.21	0.13	3.9	1,108,003
4	60	0.14	ND[b]	ND	328,375
5	87	0.03	0.04	1.0	201,207
6	92	0.03	0.17	11.1	90,831
7	92	0.03	0.03	1.4	135,514
8	112	0.30	0.23	0.2	325,202

[a] Twenty-nine mice inoculated with R5-tropic $HIV\text{-}1_{JRCSF}$ (n = 11), X4-tropic $HIV\text{-}1_{MNp}$ (n = 10), or X4-tropic $HIV\text{-}1_{NL4\text{-}3}$ (n = 8) were sacrificed 161 to 249 days after HSC transplantation. Fifteen uninfected control mice were sacrificed 174 to 249 days after transplantation, and results for the control group are expressed as means ± standard deviations.

[b] ND, not determined because of a lack of cells.

observations were similar to those seen in irradiated mice as shown in our previous report (22). Thus, humanized NOG (hNOG) mice without any myeloablation procedures allowed sufficient development of human cells to study HIV-1 pathogenesis.

hNOG mice induced systemic and long-lasting HIV-1 infection with $CD4^+$ T-cell depletion. We prepared 29 stem cell-transplanted hNOG mice and inoculated them intravenously with a high dose of R5-tropic $HIV\text{-}1_{JRCSF}$ (65,000 50% tissue culture infective doses [$TCID_{50}$]), X4-tropic $HIV\text{-}1_{MNp}$ (20,000 $TCID_{50}$), or X4-tropic $HIV\text{-}1_{NL4\text{-}3}$ (60,000 $TCID_{50}$) at 122 to 150 days posttransplantation. Then, plasma viral RNA copy numbers were measured at successive time points. The mice showed marked, long-lasting viremia state for more than 3 months, reaching the highest levels of 3.0×10^5 copies/ml from $HIV\text{-}1_{JRCSF}$-infected mice, 3.7×10^6 copies/ml from $HIV\text{-}1_{MNp}$-infected mice, and 7.8×10^6 copies/ml from $HIV\text{-}1_{NL4\text{-}3}$-infected mice (Fig. 2A). None of the mice weakened or died as a result of HIV-1 infection throughout the entire follow-up period.

All the mice were sacrificed within 4 months postinfection, and the percentages of $CD4^+$ and $CD8^+$ cells in lymphoid tissues were analyzed by flow cytometry. In a representative HIV-1-infected mouse, as shown in Fig. 2B, CD4/CD8 ratios in blood and spleen significantly decreased with apparent loss of $CD4^+$ $CD8^+$ double positive thymocytes. The size of lymphoid tissues, such as thymus and lymph node (LN), in the HIV-1-infected mice was very small compared with uninfected mice (Fig. 2C), suggesting that they shrank as a result of HIV-1 infection. Table 1 illustrates the overall profile of CD4/CD8 ratios in blood and spleen and the percentages of $CD4^+$ $CD8^+$ thymocytes from the 29 HIV-1-infected mice. Most of the mice, both R5- and X4-tropic and HIV-1 infected, had reduced CD4/CD8 ratios in blood and spleen compared with unin-

TABLE 2. Comparison of DNA proviral copies in various organs from HIV-1-infected mice[a]

Organ	No. of HIV-1 DNA copies/100 ng DNA in mice infected with[b]:		
	HIV-1_{JRCSF}	HIV-1_{MNp}	HIV-1_{NL4-3}
Peripheral blood	60	6	UD
Spleen	793	1,143	2,115
Bone marrow	2,432	656	584
Thymus	23	2,074	17,374
Lymph node	2,103	942	2,115
Lung	239	145	177
Liver	74	49	12
Small intestine	ND	6	9
Ovary	24	122	10
Uterus	14	5	16
Rectum	UD	16	11
Heart	9	UD	UD
Skin	UD	UD	138
Brain	UD	2	UD
Eyeball	3	25	UD

[a] Viral DNA was extracted from various organs of mice infected with HIV-1_{JRCSF} (33 days postinfection), HIV-1_{MNp} (59 days postinfection), and HIV-1_{NL4-3} (60 days postinfection). Determination of HIV-1 DNA copy numbers was performed by real-time PCR assay as previously described (22).

[b] UD, undetected; ND, not done.

fected control mice. On the other hand, a reduction of $CD4^+$ $CD8^+$ thymocytes was observed especially in X4-tropic HIV-1-infected mice, which seemed to correlate with the predominant expression of CXCR4 on the thymocytes as we previously described (22). Interestingly, two mice that were infected with HIV-1_{MNp} (mouse identification number 5 and 8) maintained their high percentages of $CD4^+$ $CD8^+$ thymocytes in spite of significant CD4/CD8 decline in their blood and spleen, suggesting no direct relationship between thymic T-cell depletion and CD4/CD8 decrease in peripheral blood or spleen by HIV-1 infection.

In one mouse from each R5- and X4-tropic HIV-infected group, HIV-1 proviral DNA copy numbers in various organs were measured by real-time PCR assay (Table 2). High HIV DNA copy numbers were detected in the spleen, BM, and LN of the R5-tropic HIV-1-infected mouse and in the thymus, spleen, and LN of the X4-tropic HIV-1-infected mice. In addition, HIV DNA copies were detectable in various other organs, including the lung, liver, ovary, and uterus. The fact that many human $CD68^+$ macrophages, the source of HIV-1 throughout the body (7, 8), were recognized in these organs (22) (Fig. 1H) may help explain the susceptibility of these organs to HIV-1.

To further investigate the progression of $CD4^+$ T-cell depletion by HIV-1 infection, 25 mice 120 to 151 days after HSC transplantation were randomly separated into groups of uninfected control mice (n = 7), HIV-1_{JRCSF}-inoculated mice (n = 7), HIV-1_{MNp}-inoculated mice (n = 5), and HIV-1_{NL4-3}-inoculated mice (n = 6), and then CD4/CD8 ratios and absolute $CD4^+$ T-cell numbers in peripheral blood were monitored at regular intervals. X4-tropic HIV-infected mice showed gradual decreases of their CD4/CD8 ratios and $CD4^+$ T-cell numbers, which eventually resulted in an almost complete depletion from peripheral blood (Fig. 2D). While $CD4^+$ T-cell depletion was also seen in R5-tropic HIV-infected mice, this was less prominent compared with X4-tropic HIV-1-infected mice (Fig. 2D). This pattern of R5- versus X4-tropic HIV-1 infection seems to correlate with the general observation that the emergence of X4-tropic HIVs accelerates $CD4^+$ T-cell decline and disease progression in HIV patients (12, 20).

In this study, we successfully prolonged the life span of hNOG mice by improving the HSC transplantation method and further clarified characteristics of HIV-1 infection in the mice including the following: (i) high levels of viremia lasting over 3 months, (ii) $CD4^+$ T-cell depletion in peripheral blood and spleen regardless of thymic T-cell loss, (iii) systemic HIV-1 infection not only in lymphoid tissues but also in various other organs, and (iv) a different rate of $CD4^+$ T-cell depletion for R5- versus X4-tropic HIV-1 strains. Recently, several studies on HIV-1 infection in $Rag2^{-/-}$ $\gamma c^{-/-}$ mice, transplanted with HSCs at birth, have also been reported (1, 2, 5, 24). The mice showed high susceptibility to both R5- and X4-tropic HIVs and long-term viremia with $CD4^+$ T-cell depletion, which is partly similar to our present results. However, the efficiency of human cell generation in $Rag2^{-/-}$ $\gamma c^{-/-}$ mice strongly depends on the dose of irradiation, and levels of chimerism in mice are not stable even receiving 550 to 750 cGy irradiation, which does eventually induces reduction of their life spans (5). In contrast, very stable engraftment of HSCs and subsequent human cell generation were noted in our hNOG mice even without any myeloablation procedures. Their long life spans and long-term human cell reconstitution allowed persistent HIV-1 infections mirroring HIV-1 infections in humans. Thus, this hNOG mouse system is a very useful tool as an advanced mouse model for the study of AIDS progression and long-term evaluation of new anti-HIV-1 drugs.

We thank Tomohiro Morio, Ken Watanabe, and Eiko Ogata of Tokyo Medical and Dental University for their helpful comments and skillful technical support. We are also grateful to Yukari Sasaki and Kazuhiro Takimoto of the National Institute of Infectious Diseases and Teruaki Tanaka and Junichi Fujita of the Nihon University School of Medicine for their management of animals. Human umbilical cord blood samples were obtained from the Tokyo Cord Blood Bank of the Nihon University School of Medicine.

This work was supported by a grant from the Ministry of Education, Culture, Sports, Science, and Technology to promote open research for young academics and specialists.

REFERENCES

1. **Baenziger, S., R. Tussiwand, E. Schlaepfer, L. Mazzucchelli, M. Heikenwalder, M. O. Kurrer, S. Behnke, J. Frey, A. Oxenius, H. Joller, A. Aguzzi, M. G. Manz, and R. F. Speck.** 2006. Disseminated and sustained HIV infection in $CD34^+$ cord blood cell-transplanted $Rag2^{-/-}$ $\gamma c^{-/-}$ mice. Proc. Natl. Acad. Sci. USA 103:15951–15956.
2. **Berges, B. K., W. H. Wheat, B. E. Palmer, E. Connick, and R. Akkina.** 2006. HIV-1 infection and CD4 T cell depletion in the humanized $Rag2^{-/-}$ $\gamma c^{-/-}$ (RAG-hu) mouse model. Retrovirology 3:76.
3. **Christianson, S. W., D. L. Greiner, R. A. Hesselton, J. H. Leif, E. J. Wagar, I. B. Schweitzer, T. V. Rajan, B. Gott, D. C. Roopenian, and L. D. Shultz.** 1997. Enhanced human $CD4^+$ T cell engraftment in beta2-microglobulin-deficient NOD-scid mice. J. Immunol. 158:3578–3586.
4. **Fais, S., C. Lapenta, S. M. Santini, M. Spada, S. Parlato, M. Logozzi, P. Rizza, and F. Belardelli.** 1999. Human immunodeficiency virus type 1 strains R5 and X4 induce different pathogenic effects in hu-PBL-SCID mice, depending on the state of activation/differentiation of human target cells at the time of primary infection. J. Virol. 73:6453–6459.
5. **Gorantla, S., H. Sneller, L. Walters, J. G. Sharp, S. J. Pirruccello, J. T. West, C. Wood, S. Dewhurst, H. E. Gendelman, and L. Poluektova.** 2007. Human immunodeficiency virus type 1 pathobiology studied in humanized BALB/c-$Rag2^{-/-}\gamma_c^{-/-}$ mice. J. Virol. 81:2700–2712.
6. **Hiramatsu, H., R. Nishikomori, T. Heike, M. Ito, K. Kobayashi, K. Katamura, and T. Nakahata.** 2003. Complete reconstitution of human lym-

phocytes from cord blood CD34$^+$ cells using the NOD/SCID/γ_c^{null} mice model. Blood **102**:873–880.
7. **Igarashi, T., C. R. Brown, Y. Endo, A. Buckler-White, R. Plishka, N. Bischofberger, V. Hirsch, and M. A. Martin.** 2001. Macrophage are the principal reservoir and sustain high virus loads in rhesus macaques after the depletion of CD4$^+$ T cells by a highly pathogenic simian immunodeficiency virus/HIV type 1 chimera (SHIV): implications for HIV-1 infections of humans. Proc. Natl. Acad. Sci. USA **98**:658–663.
8. **Igarashi, T., O. K. Donau, H. Imamichi, M. J. Dumaurier, R. Sadjadpour, R. J. Plishka, A. Buckler-White, C. Buckler, A. F. Suffredini, H. C. Lane, J. P. Moore, and M. A. Martin.** 2003. Macrophage-tropic simian/human immunodeficiency virus chimeras use CXCR4, not CCR5, for infections of rhesus macaque peripheral blood mononuclear cells and alveolar macrophages. J. Virol. **77**:13042–13052.
9. **Ito, M., H. Hiramatsu, K. Kobayashi, K. Suzue, M. Kawahata, K. Hioki, Y. Ueyama, Y. Koyanagi, K. Sugamura, K. Tsuji, T. Heike, and T. Nakahata.** 2002. NOD/SCIDγ_c^{null} mouse: an excellent recipient mouse model for engraftment of human cells. Blood **100**:3175–3182.
10. **Kaneshima, H., L. Su, M. L. Bonyhadi, R. I. Connor, D. D. Ho, and J. M. McCune.** 1994. Rapid-high, syncytium-inducing isolates of human immunodeficiency virus type 1 induce cytopathicity in the human thymus of the SCID-hu mouse. J. Virol. **68**:8188–8192.
11. **Kollet, O., A. Peled, T. Byk, H. Ben-Hur, D. Greiner, L. Shultz, and T. Lapidot.** 2000. β2 Microglobulin-deficient (B2m^{null}) NOD/SCID mice are excellent recipients for studying human stem cell function. Blood **95**:3102–3105.
12. **Koot, M., I. P. Keet, A. H. Vos, R. E. de Goede, M. T. Roos, R. A. Coutinho, F. Miedema, P. T. Schellekens, and M. Tersmette.** 1993. Prognostic value of HIV-1 syncytium-inducing phenotype for rate of CD4$^+$ cell depletion and progression to AIDS. Ann. Intern. Med. **118**:681–688.
13. **Koyanagi, Y., Y. Tanaka, J. Kira, M. Ito, K. Hioki, N. Misawa, Y. Kawano, K. Yamasaki, R. Tanaka, Y. Suzuki, Y. Ueyama, E. Terada, T. Tanaka, M. Miyasaka, T. Kobayashi, Y. Kumazawa, and N. Yamamoto.** 1997. Primary human immunodeficiency virus type 1 viremia and central nervous system invasion in a novel hu-PBL-immunodeficient mouse strain. J. Virol. **71**:2417–2424.
14. **Matsumura, T., Y. Kametani, K. Ando, Y. Hirano, I. Katano, R. Ito, M. Shiina, H. Tsukamoto, Y. Saito, Y. Tokuda, S. Kato, M. Ito, K. Motoyoshi, and S. Habu.** 2003. Functional CD5$^+$ B cells develop predominantly in the spleen of NOD/SCID/γc^{null} (NOG) mice transplanted either with human umbilical cord blood, bone marrow, or mobilized peripheral blood CD34$^+$ cells. Exp. Hematol. **31**:789–797.
15. **McCune, J., H. Kaneshima, J. Krowka, R. Namikawa, H. Outzen, B. Peault, L. Rabin, C. C. Shih, E. Yee, M. Lieberman, I. Weissman, and L. Shultz.** 1991. The SCID-hu mouse: a small animal model for HIV infection and pathogenesis. Annu. Rev. Immunol. **9**:399–429.
16. **Mosier, D. E., R. J. Gulizia, S. M. Baird, D. B. Wilson, D. H. Spector, and S. A. Spector. 1991.** Human immunodeficiency virus infection of human-PBL-SCID mice. Science **251**:791–794.
17. **Mosier, D. E., R. J. Gulizia, P. D. MacIsaac, B. E. Torbett, and J. A. Levy.** 1993. Rapid loss of CD4$^+$ T cells in human-PBL-SCID mice by noncytopathic HIV isolates. Science **260**:689–692.
18. **Namikawa, R., H. Kaneshima, M. Lieberman, I. L. Weissman, and J. M. McCune.** 1988. Infection of the SCID-hu mouse by HIV-1. Science **242**: 1684–1686.
19. **Shultz, L. D., P. A. Schweitzer, S. W. Christianson, B. Gott, I. B. Schweitzer, B. Tennent, S. McKenna, L. Mobraaten, T. V. Rajan, D. L. Greiner, et al.** 1995. Multiple defects in innate and adaptive immunologic function in NOD/LtSz-scid mice. J. Immunol. **154**:180–191.
20. **Tersmette, M., R. A. Gruters, F. de Wolf, R. E. de Goede, J. M. Lange, P. T. Schellekens, J. Goudsmit, H. G. Huisman, and F. Miedema.** 1989. Evidence for a role of virulent human immunodeficiency virus (HIV) variants in the pathogenesis of acquired immunodeficiency syndrome: studies on sequential HIV isolates. J. Virol. **63**:2118–2125.
21. **Ueda, T., H. Yoshino, K. Kobayashi, M. Kawahata, Y. Ebihara, M. Ito, S. Asano, T. Nakahata, and K. Tsuji.** 2000. Hematopoietic repopulating ability of cord blood CD34$^+$ cells in NOD/Shi-*scid* mice. Stem Cells **18**:204–213.
22. **Watanabe, S., K. Terashima, S. Ohta, S. Horibata, M. Yajima, Y. Shiozawa, M. Z. Dewan, Z. Yu, M. Ito, T. Morio, N. Shimizu, M. Honda, and N. Yamamoto.** 2007. Hematopoietic stem cell-engrafted NOD/SCID/IL2Rγ^{null} mice develop human lymphoid systems and induce long-lasting HIV-1 infection with specific humoral immune responses. Blood **109**:212–218.
23. **Yahata, T., K. Ando, Y. Nakamura, Y. Ueyama, K. Shimamura, N. Tamaoki, S. Kato, and T. Hotta.** 2002. Functional human T lymphocyte development from cord blood CD34$^+$ cells in nonobese diabetic/Shi-*scid*, IL-2 receptor γ null mice. J. Immunol. **169**:204–209.
24. **Zhang, L., G. I. Kovalev, and L. Su.** 2007. HIV-1 infection and pathogenesis in a novel humanized mouse model. Blood **109**:2978–2981.

JOURNAL OF VIROLOGY, Jan. 2007, p. 677–688 Vol. 81, No. 2
0022-538X/07/$08.00+0 doi:10.1128/JVI.00870-06

Nuclear Import of the Preintegration Complex Is Blocked upon Infection by Human Immunodeficiency Virus Type 1 in Mouse Cells[▽]

Naomi Tsurutani,[1]† Jiro Yasuda,[1,2] Naoki Yamamoto,[3] Byung-Il Choi,[1] Motohiko Kadoki,[1] and Yoichiro Iwakura[1]*

Center for Experimental Medicine, Institute of Medical Science, University of Tokyo, Tokyo 108-8639,[1] Fifth Biology Section for Microbiology, Department of First Forensic Science, National Research Institute of Police Science, Kashiwa 277-0882,[2] and Department of Molecular Virology, School of Medicine, Tokyo Medical and Dental University, Tokyo 113-8510,[3] Japan

Received 28 April 2006/Accepted 17 October 2006

Mouse cells do not support human immunodeficiency virus type 1 (HIV-1) replication because of host range barriers at steps including virus entry, transcription, RNA splicing, polyprotein processing, assembly, and release. The exact mechanisms for the suppression, however, are not completely understood. To elucidate further the barriers against HIV-1 replication in mouse cells, we analyzed the replication of the virus in lymphocytes from human CD4/CXCR4 transgenic mice. Although primary splenocytes and thymocytes allowed the entry and reverse transcription of HIV-1, the integration efficiency of the viral DNA was greatly reduced in these cells relative to human peripheral blood mononuclear cells, suggesting an additional block(s) before or at the point of host chromosome integration of the viral DNA. Preintegration processes were further analyzed using HIV-1 pseudotyped viruses. The reverse transcription step of HIV-1 pseudotyped with the envelope of murine leukemia virus or vesicular stomatitis virus glycoprotein was efficiently supported in both human and mouse cells, but nuclear import of the preintegration complex (PIC) of HIV-1 was blocked in mouse cells. We found that green fluorescent protein (GFP)-labeled HIV-1 integrase, which is known to be important in the nuclear localization of the PIC, could not be imported into the nucleus of mouse cells, in contrast to human cells. On the other hand, GFP-Vpr localized exclusively to the nuclei of both mouse and human cells. These observations suggest that, due to the dysfunction of integrase, the nuclear localization of PIC is suppressed in mouse cells.

A small animal model for AIDS would provide a valuable tool for the study of its pathogenesis and the evaluation of vaccine candidates and antiviral drugs. However, attempts to produce small animal models have been hampered thus far by species-specific host range barriers to infection by human immunodeficiency virus type 1 (HIV-1). CD4, the cellular receptor for HIV-1 (41, 49), was first identified as a host range barrier because mouse CD4 (muCD4) does not bind HIV-1 Env (46). Human CD4 (huCD4) transgenic (Tg) mice, however, were not susceptible to HIV-1 infection, suggesting the presence of additional barriers (47). Chemokine receptors were later identified as entry coreceptors (9, 22), but primary lymphocytes from mice transgenic for huCD4 and either huCXCR4 (70) or huCCR5 (13) exhibited little to no signs of productive infection.

Cyclin T1 (CycT1) is responsible for a transcriptional level barrier (3, 4, 26, 30, 58). CycT1 protein is a component of the TAK/pTEFb transcription factor complex (51, 78), and huCycT1 binds Tat and activates transcription from the promoter in the long terminal repeat (LTR). However, muCycT1 cannot bind Tat. Nevertheless, introduction of the huCycT1 protein to rodent cells together with a mixture of human receptors was insufficient to induce productive viral infection (11, 52).

Additional barriers have been reported in the late steps of the viral life cycle (11, 27, 40, 42, 43, 53). These late-stage defects can be rescued by fusing HIV-1-infected rodent cells to uninfected human cells (11, 52), indicating that the defects are due to the lack of necessary factors in rodent cells rather than the presence of dominant inhibitors of HIV-1 replication. CRM1, a nuclear export factor that functions in association with Rev, and p32, a splicing inhibitor and Rev-binding protein, are suggested to be necessary late-phase factors (67, 83).

We previously produced Tg mice carrying the HIV-1 proviral genome in which the *pol* gene is deleted (HIV-Tg) (36). Although transgene expression in lymphoid tissues is barely detectable under normal physiological conditions, relatively high levels of p24 Gag protein were detected in the serum (up to 400 pg/ml) after injection of bacterial lipopolysaccharide (74). All mRNA species, including unspliced, singly spliced, and multiply spliced mRNAs were produced normally. Thus, once the viral genome is integrated into the host chromosome, viral genes are expressed at a reasonable efficiency even in mouse cells, suggesting that the major host range barriers are present in the early stage of infection (prior to viral DNA integration) rather than in the late stage. However, it is not yet known whether there are any additional host range barriers in the early steps.

* Corresponding author. Mailing address: Center for Experimental Medicine, Institute of Medical Science, University of Tokyo, 4-6-1 Shirokanedai, Minato-ku, Tokyo 108-8639, Japan. Phone: 81 3 5449 5536. Fax: 81 3 5449 5430. E-mail: iwakura@ims.u-tokyo.ac.jp.

† Present address: Laboratory of Viral Infection II, Kitasato Institute for Life Sciences, Kitasato University, Tokyo 108-8641, Japan.

▽ Published ahead of print on 1 November 2006.

In this report, we investigated additional barrier steps of HIV-1 replication in mouse cells and found that the efficiency of viral genome integration into the host chromosome was low in huCD4/CXCR4 Tg mice. As this result suggested an additional barrier in the early steps of viral infection, we examined nuclear transport of the viral genome and demonstrated that integrase (IN)-dependent nuclear import of the preintegration complex (PIC) is blocked in mouse cells.

MATERIALS AND METHODS

Transgene construction. The huCD4 Tg vector (pCT4) was constructed as follows. The 0.85-kb XhoI-EcoRV fragment containing the muCD4 enhancer/promoter was ligated to a 1.8-kb EcoRV-HindIII fragment containing the huCD4 open reading frame, and then a 1.95-kb HindIII-SpeI fragment containing a rabbit β-globin intron sequence and a simian virus 40 (SV40) polyadenylation [poly(A)] signal was inserted into the HindIII-SpeI site downstream of the huCD4 gene (29) (Fig. 1A). To construct the huCXCR4 Tg vector, an XhoI-NotI fragment containing the entire coding region of huCXCR4 was isolated from pBCMGSNeo/HM89 (61), and the huCXCR4 fragment was blunted by T4 DNA polymerase, followed by insertion into the EcoRV site of pCDGH. pCDGH consisted of the muCD4 enhancer/promoter and a human growth hormone gene with its poly(A) signal but devoid of its initiation codon (pCFG) (80) (Fig. 1A). The XhoI-SpeI fragment from pCT4 and the XhoI-NotI fragment from pCFG were then purified and coinjected into the male pronuclei of fertilized mouse eggs (C3H/HeN) (80). The transgenes were detected by dot blot hybridization using DNA prepared from mouse tails (34). Mice were kept under specific-pathogen-free conditions in an environmentally controlled clean room at the Center for Experimental Medicine, the Institute of Medical Science, the University of Tokyo. All equipment and supplies were sterilized, including the cages, water bottles, wood chips, and food pellets. All experiments were conducted according to the institutional ethical and safety guidelines for animal experiments and safety guidelines for gene manipulation experiments.

Northern blot hybridization. Northern blot analyses were carried out as previously described (80). The EcoRV-SpeI fragment of huCD4 and the XhoI-NotI fragment of huCXCR4 used for transgene construction were used as templates to make probes detecting huCD4 and huCXCR4 mRNA, respectively. The autoradiograms were developed, and the radioactivity of each band was quantified with a BAS 2000 Bio-Image analyzer (Fuji Film, Tokyo, Japan).

Plasmids. The HIV-1 pNL4-3 (X4-tropic, accession no. M19921) vector was obtained from A. Adachi (1). The HIV-1 pNL43lucΔenv vector, in which the *env* gene is defective and the *nef* gene is replaced by the firefly luciferase (*Luc*) gene, the pNL4-3 vector containing a mutation at the IN catalytic site (D116G), and an amphotropic Moloney murine leukemia virus (MuLV) envelope expression vector (pJD-1) were kindly provided by T. Masuda (54, 65, 76). A vesicular stomatitis virus G (VSV-G)-expressing plasmid (pMD-G) was obtained from L. Naldini (5, 62). The pGEM/NL-2-LTR plasmid was kindly provided by Y. Koyanagi (73).

The HIV-1 pNL43lucΔenv vector carrying a IN protein tagged with the SV40 nuclear localization signal (NLS) was constructed by using overlap extension PCR (33). First, two different PCRs were performed using HIV-1 pNL43lucΔenv vector as the template: one with the AflII-sense primer, 5'-CATCTTAAGACA GCAGTACAAATGGCAGTA-3', and NLS-antisense primer, 5'-GGCCTTTC TCTTCTTTTTTGGATCCTCATCCTGTCTACTTGCC-3', and the other with the NLS-sense primer, 5'-CCAAAAAAGAAGAGAAAGGCCTAACACATG GAAAAGATTAGT-3', and PflMI-antisense primer, 5'-CTCTTTTTCCTCCA TTCTATGGAGACTCCCTG-3'. These two PCR amplicons were then combined and used as the template for the third PCR with outer primers AflII-sense and PflMI-antisense. The final PCR product was digested with AflII and PflMI and ligated to the SpeI/AflII and SpeI/PflMI vector fragments of HIV-1 pNL43lucΔenv. The nucleotide sequence of the construct was confirmed by sequencing.

To prepare the expression vector for HIV-1 IN N-terminal fusion to enhanced green fluorescence protein (EGFP) (GFP-IN), the entire coding region of HIV-1 IN was amplified by PCR and inserted into the pEGFP-C2 expression vector (Clontech Laboratories, Palo Alto, CA) at its EcoRI and ApaI sites. The primers used to amplify the HIV IN were GFP-IN-sense, 5'-CCGGAATTCCGGGCC ATAGCGGCCTTTTTAGATGGAATAGAT-3', and GFP-IN-antisense, 5'-TC CGGGCCCGGATTAATCCTCATCCTGTCTACT-3'. To generate the expression vector for the HIV-1 Vpr N or C terminus fused to EGFP (GFP-Vpr, Vpr-GFP), the entire coding region of HIV-1 Vpr was amplified by PCR and inserted into the pEGFP-C2 or pEGFP-N1 expression vector at the HindIII and ApaI or HindIII and BamHI sites, respectively. The primers used to amplify HIV-1 Vpr were GFP-Vpr-sense, 5'-CCCAAGCTTGGGGGACGCCATGGA ACAAGCCCCAGAA-3', and GFP-Vpr-antisense, 5'-TCCGGGCCCGGACT AGGATCTACTGGCTCCATT-3', or Vpr-GFP-sense, 5'-CCCAAGCTTGGG GACATGGAACAAGCCCCAGAA-3', and Vpr-GFP-antisense, 5'-CGCGGA TCCGCGGAGGATCTACTGGCTCCATT-3', respectively. The amplified regions and the cloning junctions were confirmed by DNA sequencing.

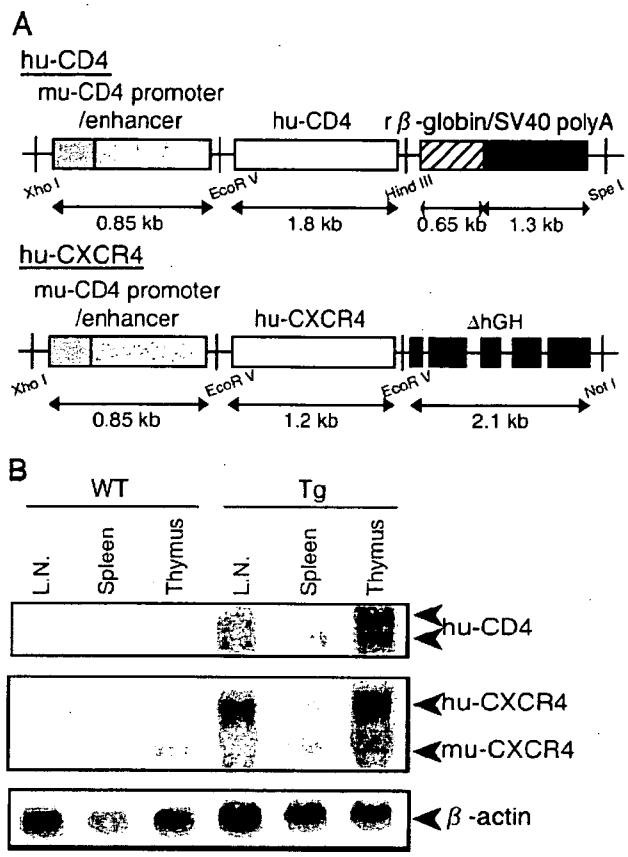

FIG. 1. (A) Transgene constructs. huCD4 or CXCR4 cDNA was placed downstream of the muCD4 enhancer/promoter and ligated to the SV40 poly(A) signal (huCD4) or to a defective human growth hormone gene containing the poly(A) signal (huCXCR4). (B) Transgene expression in lymphatic organs. Northern blot hybridization analysis was performed using 10 μg of total RNA prepared from the thymus, spleen, or lymph nodes of WT or Tg mice. The positions expected for huCD4, huCXCR4, muCXCR4, and β-actin mRNA are indicated on the right.

Cell culture and isolation of human PBMCs and mouse splenocytes and thymocytes. Human fibroblast-like cell lines (293T and HeLa), a mouse embryo fibroblast-like cell line (NIH 3T3) derived from an NIH Swiss mouse (Fv-1^n), and a mouse rectum carcinoma cell line (Colon-26) from a BALB/c mouse (Fv-1^b) were cultured in Dulbecco's modified Eagle's medium (Invitrogen, Tokyo, Japan) supplemented with 10% fetal bovine serum (FBS). The Colon-26 cell line was obtained provided from the Cell Resource Center for Biomedical Research Institute of Development, Aging, and Cancer, Tohoku University, Japan (75). Human T-cell lymphoma cell lines (MT-4 and Jurkat) and mouse T-cell lymphoma cell lines (EL4, YAC-1, and BW5147) were cultured in RPMI 1640 (SIGMA, Tokyo, Japan) containing 10% FBS. Human peripheral blood mononuclear cells (PBMCs) were obtained from peripheral blood. Briefly, buffy coats from the peripheral blood of healthy HIV-seronegative blood donors were separated over a Ficoll-Hypaque gradient (Ficoll-Paque PLUS; GE Healthcare Bio-Sciences, Tokyo, Japan). C3H/HeN mice (Charles River, Tokyo, Japan) were sacrificed at 8 weeks, and the splenocytes and thymocytes were isolated by passage through nylon mesh. Human PBMC suspensions and mouse splenocytes

and thymocytes were stimulated with 1% phytohemagglutinin (SIGMA, Tokyo, Japan). These cells were grown in RPMI 1640 medium containing 4 ng/ml of recombinant human interleukin 2 or mouse interleukin 2 (Peprotech EC Ltd, London, United Kingdom) per ml and 10% FBS. After 1 week, human PBMCs and mouse splenocytes and thymocytes were >96% T cells and >40% activated cells, as judged by fluorescence-activated cell sorter analysis using anti-CD3 or anti-CD69 monoclonal antibodies (BD Biosciences, Tokyo, Japan), respectively (data not shown).

Virus preparation and infection assays. HIV-1 strain NL4-3 was propagated in MT-4 cells, and the supernatants were filtered and stored at −80°C until use. For single-round infection assays, pseudotyped viruses were generated by cotransfection of 293T cells with pNL43lucΔenv vector and an amphotropic Moloney MuLV envelope expression vector (pJD-1) or a VSV-G envelope expression vector (pMD-G) using Lipofectamine PLUS (Invitrogen) (76). The pNL43lucΔenv vector containing a mutation at the IN catalytic site (D116G) was used as a control (54). The culture supernatants of the transfected 293T cells were harvested at 48 h posttransfection, filtered through 0.45-μm filters, and used as the virus preparations. Each virus preparation was treated with DNase I (40 μg/ml; Worthington Biochemical Co., Lakewood, NJ) in the presence of 10 mM $MgCl_2$ at 37°C for 1 h to avoid DNA contamination. An aliquot of each virus preparation was incubated at 65°C for 1 h and used as a heat-inactivated control. To monitor viral gene expression from the pNL43lucΔenv vector carrying a IN protein tagged with the SV40 NLS, luciferase activity in transfected 293T cells was measured on a Lumat LB9507 luminometer (BERTHOLD, Technologies, Bad Wildbad, Germany). At 48 h posttransfection, 293T cells were lysed with 1 ml of luciferase lysis buffer (Promega). One microliter of each cell lysate was subjected to the luciferase assay. Human PBMCs (5×10^6) or HeLa (5×10^5), MT-4 (5×10^6), Jurkat (5×10^6), mouse splenocytes (5×10^6), mouse thymocytes (5×10^6), NIH 3T3 (5×10^5), BW5147 (5×10^6), EL4 (5×10^6), or YAC-1 (5×10^6) cells were infected with an aliquot (2 ml; containing approximately 500 ng [NL4-3], 200 ng [HIV-1/MuLV], or 50 ng [HIV-1/VSV-G] of p24) of DNase-treated virus. The infection proceeded in the presence of Polybrene (SIGMA, Tokyo, Japan) (10 μg/ml) at 37°C. After 6 h, the viruses were removed, and the cells were overlaid with fresh media and incubated at 37°C. For p24 CA analysis, the infected cell supernatants were removed on the indicated days following infection. The levels of HIV-1 p24 antigen were determined by an enzyme immunoassay system (RETRO-TEK; ZeptoMetrix Corp., Buffalo, NY). For luciferase analysis, infected cells were harvested 4 days after infection, and the total cell pellets from each well were washed twice with phosphate-buffered saline (PBS) and lysed in luciferase lysis buffer (Promega). Luciferase activity (measured in a relative light units [RLU]) was measured on a Lumat LB9507 luminometer (BERTHOLD, Technologies, Bad Wildbad, Germany).

Analysis of HIV-1 DNA synthesis and formation of 2-LTR circles. Cells were harvested 24 h after infection. After washing with PBS, nucleic acids were extracted as described previously (81). Briefly, cells were disrupted in urea lysis buffer (4.7 M urea, 1.3%, sodium dodecyl sulfate [SDS], 0.23 M NaCl, 0.67 mM EDTA, and 6.7 mM Tris-HCl [pH 8.0]), phenol-chloroform extracted, and ethanol precipitated. The DNA pellet was resuspended in distilled H_2O, and an aliquot of each sample was analyzed by PCR. For ex vivo infection of primary lymphocytes from huCD4/CXCR4 Tg mice, partial reverse transcripts of the viral DNA were quantified by semiquantitative PCR. The primers used were as follows (37, 45, 81): R-U5, R, 5′-GCCTCAATAAAGCTTGCCTTG-3′ (sense, positions 522 to 542); U5, 5′-CCACTGCTAGAGATTTTCCAC-3′ (antisense, positions 616 to 638); Gag forward, 5′-TGGGGGGACATCAAGCAGCCATG CA-3′ (sense, positions 1360 to 1385); Gag reverse, 5′-CTATGTCACTTCCCC TTGGTTCTCT-3′ (antisense, positions 1474 to 1498). The PCR program was 30 cycles at 95°C for 1 min, 60°C for 1 min, and 72°C for 1 min in the presence of [^{32}P]dCTP. The PCR products were electrophoresed on an 8% polyacrylamide–Tris-borate-EDTA gel. The autoradiograms were developed, and the radioactivity of each band was quantified by a BAS 2000 Bio-Image analyzer. For single-round infections, the DNA was measured by quantitative PCR using an ABI PRISM 7900HT qPCR machine (Applied Biosystems, Tokyo, Japan). The PCR primer pairs were as follows: R-U5 (M667/AA55), R-gag (M667/M661) (76), and the 2-LTR junction's sequence (2-LTR-S/2-LTR-AS) (73). The cycling conditions included a hot start (50°C for 2 min, 95°C for 10 min), followed by 40 cycles of denaturation (95°C for 15 s) and extension (60°C for 1 min). To compensate for varying DNA sample recovery, the data are presented as ratios of HIV-1 DNA to β-actin DNA.

Cassette ligation-mediated PCR and integration analysis. For the detection of the HIV-1 integration form, we designed a cassette ligation-mediated PCR system using an in vitro LA cloning kit (TaKaRa BIO, Shiga, Japan) (35) (see Fig. 3A). Briefly, 5 μg of DNA was digested with EcoRI and ligated to double-stranded DNA cassettes with compatible ends. The cassette-ligated restriction fragments were then subjected to two rounds of PCR using the cassette- and HIV-specific primers C1 (5′-GTACATATTGTCGTTAGAACGCGTAATACG ACTCA-3′) and Gag reverse (described above) for the cassette, *gag*, and its upstream region and C2 (5′-CGTTAGAACGCGTAATACGACTCACTATAG GGAGA-3′) and U5 reverse (described above) for the cassette sequence downstream of C1 and the LTR region. PCR was performed according to the manufacturer's instructions. The amplification conditions were 30 cycles of 1 min at 94°C, 2 min at 54°C, 2 min at 72°C, and a final extension of 1 min at 72°C. The amplified products were resolved on 2% agarose gels and stained with SYBR green (FMC Bioproduct, Rockland, ME).

Fluorescence microscopy. HeLa (4×10^4), NIH 3T3 (3×10^4), and Colon-26 (3×10^4) cells were seeded onto 8-well culture slides (Nalge Nunc International, Rochester, NY) and transfected with the indicated plasmids using Lipofectamine 2000 (Invitrogen). At 24 h posttransfection, the cells were washed once in PBS and fixed with acetone for 5 min. After washing with PBS, the cells were mounted in 90% glycerol–50 mM $NaHCO_3$-Na_2CO_3 and covered by a coverslip. Confocal microscopy was performed with a Nikon Optiphot-2 fluorescence microscope with a Bio-Rad MRC 1024 laser confocal imaging system, and the digital images were prepared using Adobe Photoshop software.

Particle preparation and Western blot analysis. The culture supernatant (5 ml) of HIV-1 producing plasmid-transfected 293T cells was collected at 48 h postinfection. It was centrifuged thorough 20% (wt/vol) sucrose–PBS in an SW55 rotor (Beckman Coulter) at 4°C at 147,000 × *g* for 2 h (56), and the pellet was resuspended in PBS. The viral pellets were hearted at 90°C for 10 min in the presence of sample buffer (62.5 mM Tris-HCl, pH 6.8, 10% glycerol, 2% SDS, 5% 2-mercaptoethanol, 0.005% bromophenol blue). Then viral proteins were electrophoresed on a 12% SDS–polyacrylamide gel containing 0.2% SDS. Following blotting of proteins onto a polyvinylidene difluoride membrane, the membrane was first incubated with an antiserum from an AIDS patient (provided by Y. Inagaki, Tokyo Medical and Dental University, Tokyo, Japan, and Y. Koyanagi, Kyoto University, Kyoto, Japan), followed by horseradish peroxidase-conjugated anti-human immunoglobulin. HIV-1 proteins were visualized using an enhanced chemiluminescence detection system (GE Healthcare Bio-Science, Tokyo, Japan).

Statistical analysis. Data were analyzed using Excel and Student's *t* test. A *P* value of <0.05 was considered statistically significant, and all results are presented as means ± standard errors of the means (SEM).

RESULTS

Lymphocytes from huCD4/CXCR4 Tg mice do not fully support HIV-1 infection. To elucidate the host range barriers of HIV-1 replication in mice, we analyzed the early processes of HIV-1 infection in huCD4/CXCR4 Tg mouse splenocytes. Transgenic mice were generated by introducing both huCD4 and huCXCR4 cDNA along with the muCD4 enhancer/promoter into fertilized C3H mouse eggs (Fig. 1A). As shown in Fig. 1B, the huCD4 and huCXCR4 mRNAs were detected mostly in the thymus but also in the lymph nodes and spleen. Two huCD4 mRNA species were detected due to alternative splicing of the SV40 gene that was ligated to the huCD4 gene (Fig. 1B). fluorescence-activated cell sorter analyses showed that Tg splenocytes and thymocytes both expressed huCD4 and huCXCR4 on their cell surfaces (data not shown).

To examine the susceptibility of these Tg mice to HIV infection, splenocytes and thymocytes were isolated from the mice and infected with T-tropic HIV-1 (NL4-3) or M-tropic HIV-1 (JR-CSF). However, we could not detect any p24 antigen in the culture supernatant of these Tg mouse-derived cells, although significant levels of p24 (up to 80 pg/ml) were produced in human PBMC culture supernatant 12 days after infection.

To determine the process by which the viral replication is blocked, we analyzed the early infection steps by examining the viral genomic structure. Twenty-four hours after HIV-1 infection of the huCD4/CXCR4 Tg splenocytes, cells were har-

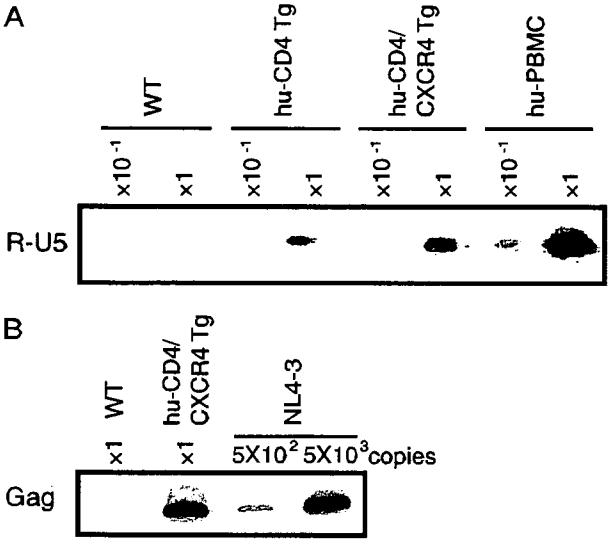

FIG. 2. HIV infection of splenocytes and thymocytes of WT and huCD4/CXCR4 Tg mice. Splenocytes or thymocytes from WT mice, Tg mice, or human PBMCs were isolated and infected with equivalent amounts of DNase-treated NL4-3 virus at 37°C for 6 h. After 6 h, the viruses were removed and the cells were treated with trypsin (500 μg/ml) at 37°C for 10 min and then washed in growth medium. (A and B) Splenocytes were harvested at 24 h postinfection. Total DNA was extracted from the cells and subjected to PCR analysis with a primer pair for R/U5 (A) or R/gag (B). The reaction was carried out using the DNA preparation from 1×10^5 cells (×1) or 1×10^4 cells ($\times 10^{-1}$). In panel B, the lanes marked 5×10^2 and 5×10^3 represent PCR products using 5×10^2 or 5×10^3 copies of the pNL4-3 plasmid as the template.

vested and total DNA was extracted. Early (R-U5) and late-infectious intermediate products (R-gag) were determined using semiquantitative PCR with specific primers. As shown in Fig. 2A and B, both infectious intermediates were detected specifically in the DNA isolated from the splenocytes of huCD4/CXCR4 Tg mice exposed to HIV-1, indicating that viral entry and reverse transcription had proceeded normally in mouse cells provided that human viral receptors were supplied. Similar results were also obtained in huCD4/CCR5 Tg mouse splenocytes infected with HIV-1 JR-CSF (data not shown). In contrast, the early infectious intermediate was not detected in wild-type mouse splenocytes, indicating a block upon viral entry. Taken together, these results suggest that HIV-1 replication in huCD4/CXCR4 Tg splenocytes was blocked later than the reverse transcription step(s).

HIV-1 infection of mouse cells is blocked at steps preceding integration into the host chromosome. We next examined the integration of the HIV-1 genome into the host chromosome. The pNL4-3 vector containing a mutation at the IN catalytic site (D116G) was used as a control (54). DNA from the infected cells was digested with EcoRI, which cut proviral DNA at only one site (nucleotide number 5743 of NL4-3, accession no. M19921). The DNA was then ligated to an EcoRI-specific cassette and subjected to the first round of PCR using primers specific for the cassette and the *gag* region, followed by the second round of PCR using primers for the cassette and the LTR region (Fig. 3A). As a result, the integrated viral DNA was visualized as smearing bands greater than 638 bp, which is

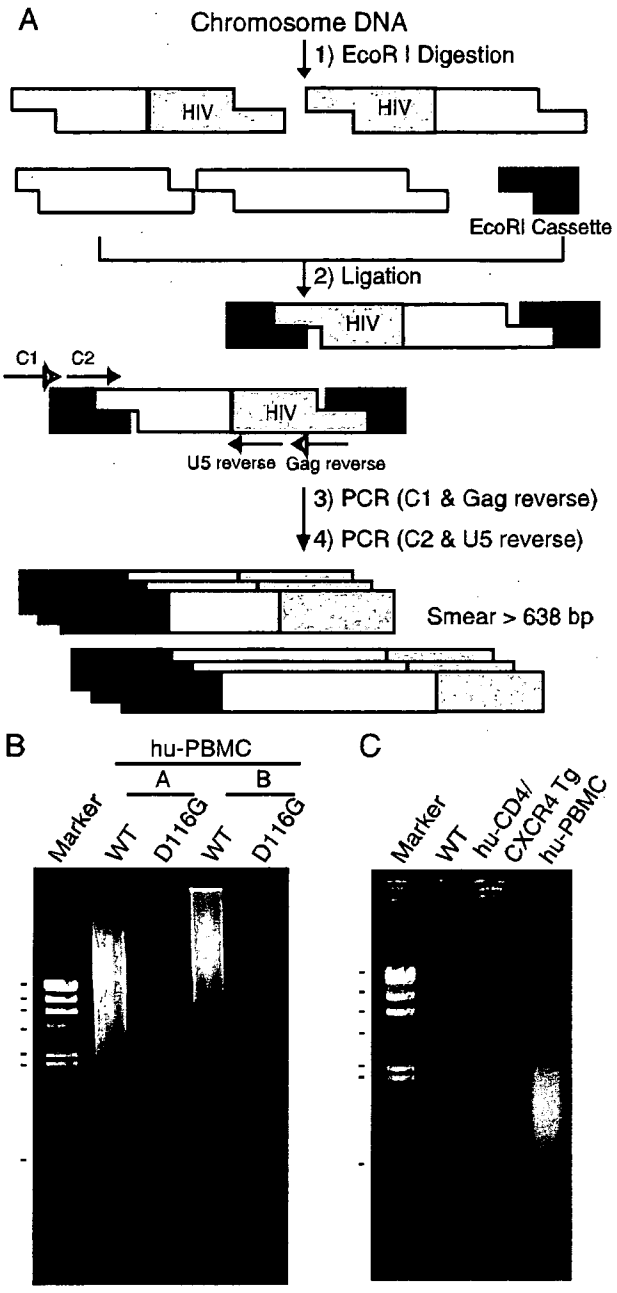

FIG. 3. Suppression of NL4-3 virus DNA integration in the mouse chromosome. Human PBMCs and murine splenocytes were infected with equivalent doses of DNase-treated NL4-3 virus. After 6 h, the virus was removed and the cells were washed with growth medium. At 1 day postinfection, the cells were harvested and used to extract total DNA. The DNA (5 μg) was digested with EcoRI and ligated to double-stranded DNA cassettes with compatible ends. The cassette-ligated DNA fragments were used as templates for nested PCR using cassette- and HIV-specific primers. (A) Schematic representation of cassette ligation-mediated PCR and the primers used to detect HIV integration into the host chromosome. (B and C) Detection of the chromosome-integrated forms of viral DNA. (B) Human PBMC preparations from two donors (A and B) were infected with NL4-3-WT or integrase mutant (D116G), and the DNAs were subjected to PCR analysis. Markers: 23.1, 9.4, 6.6, 4.3, 2.3, 2.0, and 0.564 kb (λ/HindIII). (C) DNA was isolated from NL4-3-infected splenocytes or thymocytes from WT or Tg mice or human PBMCs following infection and subjected to PCR analysis. Note the smearing bands in virus-infected human PBMCs but not in huCD4/CXCR4 Tg mice. Marker: λ/HindIII.

the original length between C2 and U5 reverse primers without insertion. Smearing bands were clearly detected when the DNA from HIV-1 wild type (WT)-infected human PBMCs was analyzed. In contrast, no smearing bands were detected with the DNA from HIV-1-D116G infected human PBMC, HIV-1-WT infected splenocytes from WT, and huCD4/CXCR4 transgenic mice (Fig. 3B and C). These results suggest that HIV-1 replication is also blocked in mouse cells at steps between the entry and viral DNA integration steps or at the viral integration step in addition to the adhesion/entry step.

The infection of mouse cells with both HIV-1/pJD-1 and HIV-1/VSV-G pseudotyped virus are blocked at a postentry step. To examine the possibility that HIV-1 replication in mouse cells is blocked at steps between the viral entry and DNA integration steps, we analyzed the early steps of viral infection using HIV-1 pseudotyped viruses in which the Env is replaced by an amphotropic MuLV Env (HIV-1/pJD-1) or by the G protein of VSV (HIV-1/VSV-G) and the *nef* gene is replaced by the firefly luciferase gene (76). The MuLV envelope pseudotype uses a ubiquitously expressed phosphate transporter as the receptor (55), and the VSV-G envelope pseudotype is capable of infecting cells through a carbohydrate receptor and the endocytic pathway (2). By using these pseudotyped viruses, we overcame the barriers at the adhesion and entry steps.

Among the adherent cells tested, 293T and HeLa cells showed high luciferase activity upon infection with both types of pseudotyped viruses, whereas NIH 3T3 cells yielded 10- to 100-fold-lower signals (Fig. 4). Similarly, the mouse T-cell lines BW5147, EL4, and YAC-1 displayed 100- to 1,000-fold-lower signals than did the human T-cell lines MT4 and Jurkat. Furthermore, luciferase expression efficiency was lower, by more than 1,000-fold, in mouse primary splenocytes than in human PBMCs. The relative sensitivity to infection of these cells was similar between the two pseudotyped viruses, although the efficiency of infection was approximately 10-fold higher in the HIV-1/VSV-G infection. Thus, these results again support a species-specific block in mouse cells subsequent to the entry step.

Reverse transcription of HIV-1 proceeds normally in mouse cells. We next evaluated the ability of mouse cells to support HIV-1 DNA synthesis. One day after infection, total DNA was harvested from various infected cells and subjected to quantitative PCR analyses. Both early (R-U5) and late (R-gag) reverse transcription products were specifically detected in DNA isolated from human and mouse cells exposed to both of the pseudotyped viruses, HIV-1/pJD-1 (Fig. 5A) and HIV-1/VSV-G (Fig. 5B). No R-U5 or R-gag products were detected when heat-inactivated (65°C, 1 h) viruses were infected, indicating that these products were not derived from the transfected HIV-1 DNA carryover. The copy number of R-U5, which reflects the efficiency of viral entry, was higher in mouse cells (NIH 3T3, BW5147, and splenocytes) than in human cells (HeLa, MT4, and PBMCs). The ratio of R-gag/R-U5 was calculated to evaluate the efficiency of the reverse transcription because R-U5 reflects the efficiency of entry (Fig. 5A and B, lower panels). No significant difference in the efficiency of reverse transcription was observed between mouse cells and human cells exposed to HIV-1/pJD-1 (Fig. 5A) and HIV-1/VSV-G (Fig. 5B). These results indicated that mouse cells supported reverse transcription at an efficiency similar to that of human cells.

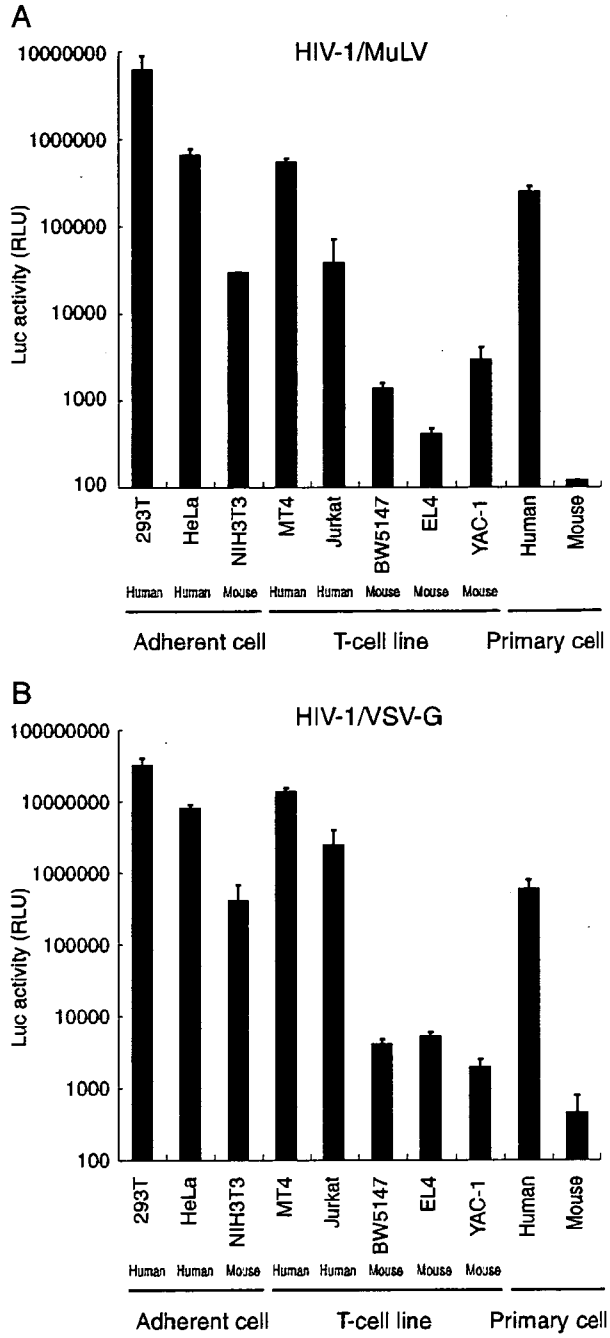

FIG. 4. Analysis of HIV-1 pseudotype virus replication in mouse cells. Human and murine cells were infected with equivalent doses of pNL43lucΔenv that was pseudotyped with either MuLV (A) or VSV-G (B) at 37°C for 6 h. After removal of the virus, cells were washed in growth medium. Luciferase activity was measured at 4 days postinfection, and normalized activities relative to the total protein quantity are shown. The data represent the means ± SEM of results from three wells. The data were reproduced in three independent experiments.

Nuclear import of the PIC is blocked in mouse cells. After completion of reverse transcription, the PIC crosses the

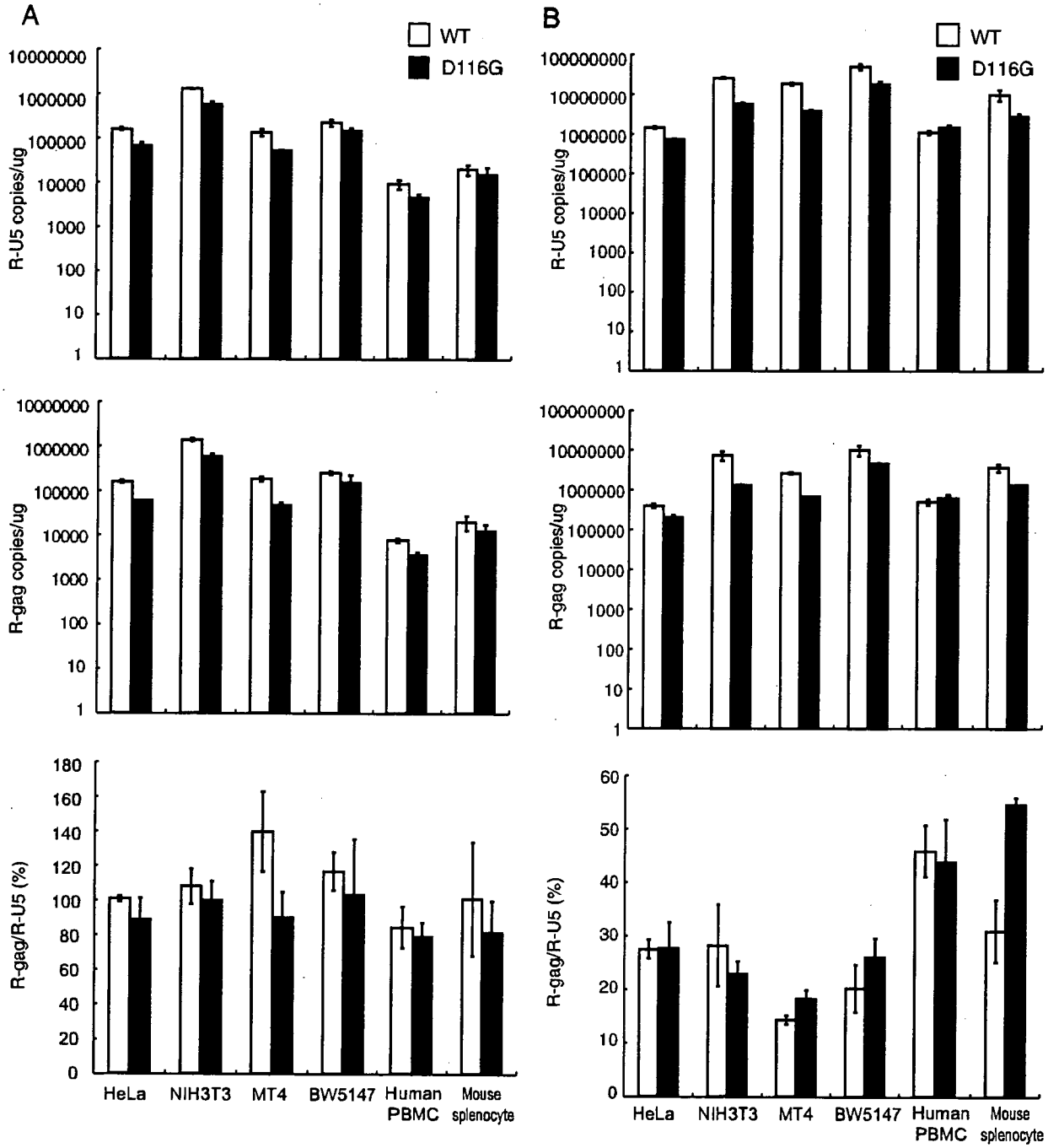

FIG. 5. The efficiency of the reverse transcription of HIV-1 in mouse cells. Human and murine cells were infected with equivalent doses of DNase-treated WT or integrase mutant (D116G) MuLV pseudotyped virus (A) or VSV-G pseudotyped virus (B). At 1 day postinfection, the cells were harvested, and the total DNA was extracted and subjected to quantitative real-time PCR analysis using primer pairs for R/U5 (upper panels) or R/gag (middle panels). The copy numbers of HIV-1 DNA per 1 μg β-actin are shown. The reverse transcription (RT) efficiency is calculated by dividing the late RT product (R-gag) by the early RT product (R-U5) (lower panel). The data represent the means ± SEM of results from three wells. The data were reproduced in three independent experiments.

nuclear membrane and enters the nucleus. Ligases within the nucleus then circularize the proviral DNA (2-LTR containing circular DNA) before its integration into the host chromosome (17, 57, 82). Although these 2-LTR circles are nonfunctional, they can serve as a measure of viral nuclear entry. To assess the efficiency of PIC transport into the nuclei of mouse cells, we estimated de novo-synthesized 2-LTR circular-form DNA by PCR using primer pairs that amplify sequences unique to this DNA form. The fragment corresponding to the 2-LTR circular junction was clearly

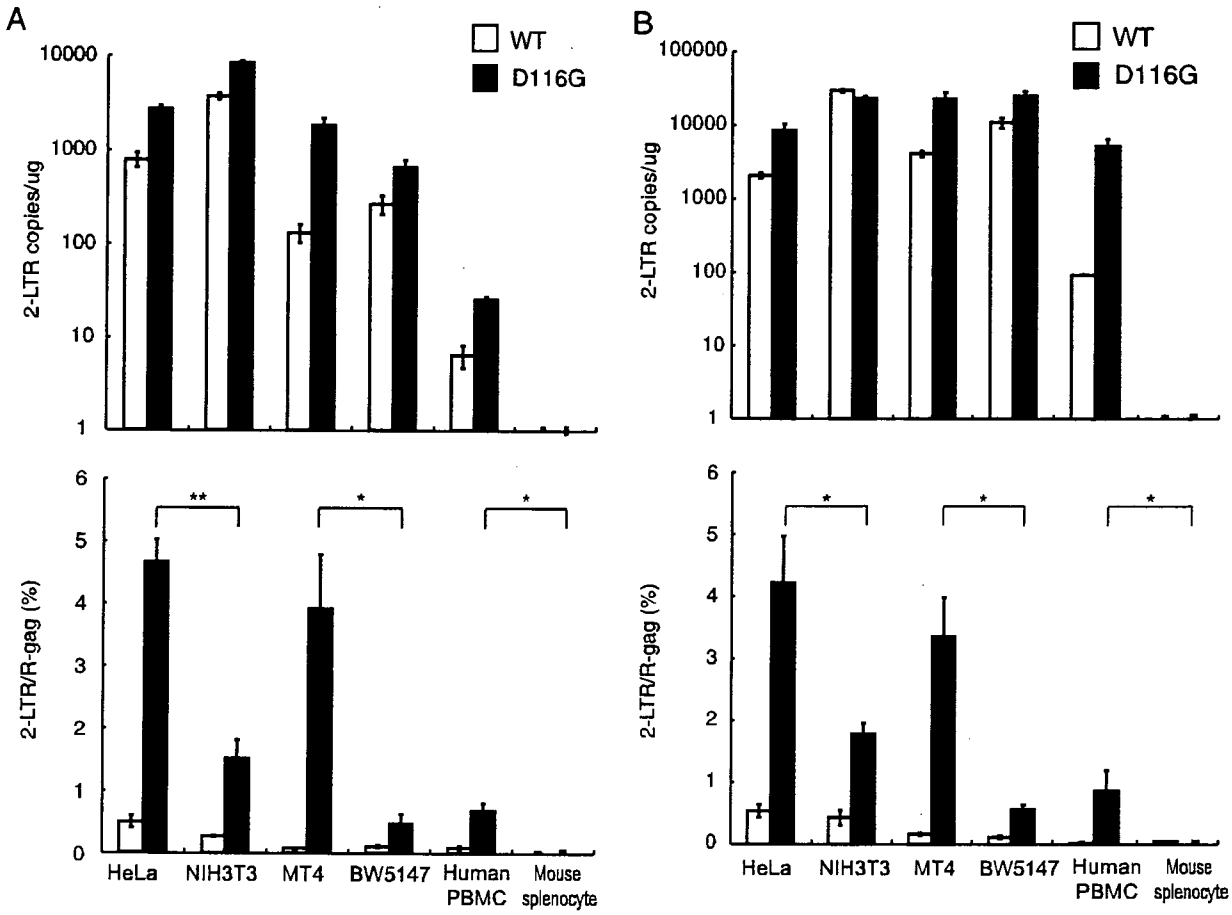

FIG. 6. Suppression of the 2-LTR circular form of DNA in mouse cells. Human and mouse cells were infected with equivalent doses of DNase-treated WT or integrase-mutant (D116G) MuLV pseudotype virus (A) or VSV-G pseudotype virus (B). The DNA from the infected cells was subjected to quantitative real-time PCR analysis using a primer pair specific for the 2-LTR circular form of the DNA (upper panels). The nuclear import efficiency was calculated by dividing the 2-LTR products by the late reverse transcription products (lower panels). The data represent the means ± SEM of results from three wells, and the data were reproduced in three independent experiments. *, $P < 0.05$; **, $P < 0.01$ (determined by Student's t test).

detected at 1 day postinfection in the DNA samples from HeLa, NIH 3T3, MT-4, BW5147, and human PBMCs infected with HIV-1/pJD-1 pseudotyped virus (Fig. 6A, upper panel). However, only a small amount of 2-LTR circle was detected in the mouse splenocytes. A similar tendency was observed in cells infected with the HIV-1/VSV-G pseudotyped virus (Fig. 6B, upper panel). The 2-LTR DNA in mouse cells was also measured at 2 and 4 days postinfection using both pseudotyped viruses and provided similar results (data not shown).

The ratio of 2-LTR/R-gag was calculated to evaluate the efficiency of nuclear import because the copy number of 2-LTR in the nucleus should be dependent on the amount of cytoplasmic R-gag, which represents the precursor of 2-LTR. The efficiency was very low and not significantly different between human and mouse when wild-type HIV-1 pseudovirus was infected (Fig. 6, lower panel). Because the nuclear concentration of 2-LTR is determined by the balance between accumulation of PIC by nuclear import and loss of PIC from the nucleoplasm by chromosome integration, we next used an integration-defective mutant, D116G, to examine only the efficiency of nuclear import. As shown in Fig. 6, the ratio was significantly lower in NIH 3T3 cells than in HeLa cells (33% or 43% of HeLa cells) and in BW5147 cells than in MT4 cells (12% or 17% of MT4 cells) when they were infected with HIV-1/pJD-1 or HIV-1/VSV-G, respectively (Fig. 6A and B, lower panels). We were unable to compare the efficiency of PIC import in human PBMCs and mouse splenocytes because the 2-LTR circle was not detected in mouse splenocytes. These results suggested that the nuclear import of the PIC is blocked in mouse cells, especially in splenocytes.

A block in the nuclear localization of the PIC is caused by a defect in IN nuclear localization. As Vpr and IN play important roles in importing the PIC into the nucleus, we hypothesized that Vpr and/or IN is nonfunctional in mouse cells due to the inability to utilize the cellular factors necessary for trafficking to the nucleus. To directly examine the karyophilic properties of HIV-1 IN in mouse cells, we generated an expression vector with HIV-1 IN in which the N terminus was fused to EGFP (GFP-IN). Since it was reported that β-galactosidase fusion to the C terminus of IN could not be located in

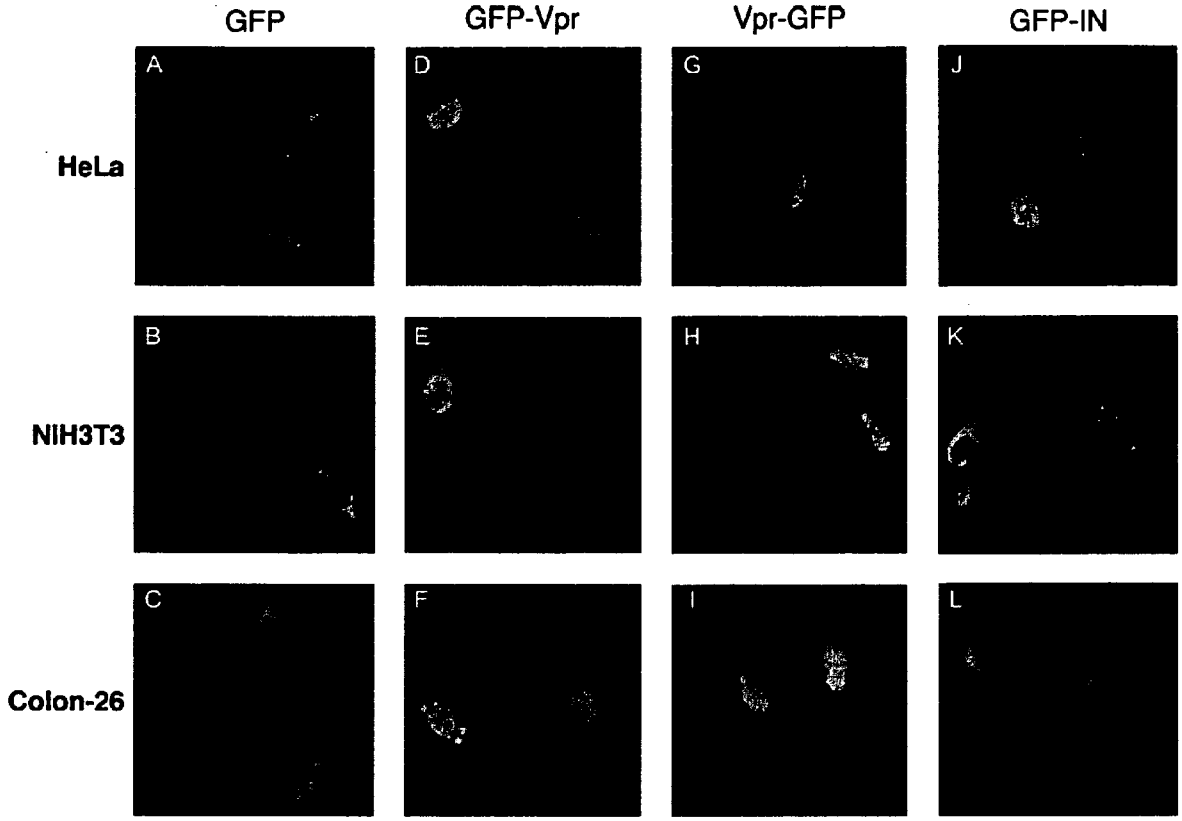

FIG. 7. Inhibition of IN-dependent GFP nuclear import in mouse cells. HeLa (A, D, G, and J), NIH 3T3 (B, E, H, and K), and Colon-26 cells (C, F, I, and L) were transfected with plasmids expressing GFP only (A, B, and C), GFP fused to the HIV-1 Vpr N terminus (GFP-Vpr) (D, E, and F), GFP fused to the HIV-1 Vpr C terminus (Vpr-GFP) (G, H, and I), and GFP fused to HIV-1 IN (J, K, and L) using Lipofectamine 2000. At 24 h posttransfection, the cells were fixed and visualized by confocal fluorescence microscopy. Note that the nuclear localization of GFP-IN is inhibited in mouse cells (K and L).

the nucleus (44), we did not examine the C terminus fusion construct (IN-GFP). We also generated HIV-1 Vpr expression vectors in which the N or C terminus was fused to EGFP (GFP-Vpr and Vpr-GFP, respectively). At 24 h postinfection, HeLa, NIH 3T3, and Colon-26 cells were transfected with the GFP fusion vectors, and the subcellular localization of IN or Vpr was examined with a confocal microscope. We used Colon-26 cells (Fv-1^n) in addition to NIH 3T3 cells (Fv-1^b) because Fv-1 may exert its antiretroviral effect at a postentry step, after reverse transcription and prior to integration (38, 79). Colon-26 cells and NIH 3T3 cells showed similar levels of luciferase activity upon infection with both types of pseudotyped viruses. Control GFP without IN or Vpr was distributed uniformly throughout both the cytoplasm and the nuclei in all cells examined (Fig. 7A to C). GFP-Vpr, on the other hand, accumulated almost exclusively in the nuclei of HeLa (Fig. 7D), NIH 3T3 (Fig. 7E), and Colon-26 (Fig. 7F) cells, although low levels of nuclear membrane association were also observed in NIH 3T3 cells (Fig. 7E). Vpr-GFP also accumulated almost exclusively in the nuclei of HeLa (Fig. 7G), NIH 3T3 (Fig. 7H), and Colon-26 (Fig. 7I) cells. These results indicated that HIV-1 Vpr has strong karyophilic properties and that, even in mouse cells, it can be transported across the nuclear membrane. In contrast, although GFP-IN accumulated almost exclusively in the nuclei of HeLa cells (Fig. 7J), GFP-IN was localized only in the cytoplasm of NIH 3T3 (Fig. 7K) and Colon-26 (Fig. 7L) cells. Thus, our results demonstrate that IN-mediated nuclear transport of HIV-1 PIC is impaired in mouse cells of both Fv-1 genotypes.

Addition of the SV40 NLS to the C terminus of HIV-1 integrase enhances viral infectivity in mouse cells. To analyze the role of IN in nuclear localization of HIV-1, we constructed an HIV-1 pNL43lucΔenv vector with the SV40 NLS at the C terminus of IN (IN-NLS), and pseudotyped virus was generated by cotransfection of 293T cells with the pNL43lucΔenv wild type or IN-NLS vector and VSV-G expression vector. Luciferase activity in the cell lysate of 293T cells transfected with IN-NLS was increased 2.5-fold compared to that transfected with wild-type virus (Fig. 8A). To verify that the gag-pol polyprotein processing was completed in IN-NLS virus particles, we performed Western blot analysis using an AIDS patient serum. No difference of the viral components was observed between parental WT and IN-NLS viruses (Fig. 8B). The content of p24 protein of the IN-NLS was also shown to be normal using a specific monoclonal antibody (data not shown). These results showed that addition of NLS to IN significantly activates viral replication.

Then we tested the susceptibility of HeLa, NIH 3T3, BW5147, and MT4 cells to IN-NLS infection. Addition of the

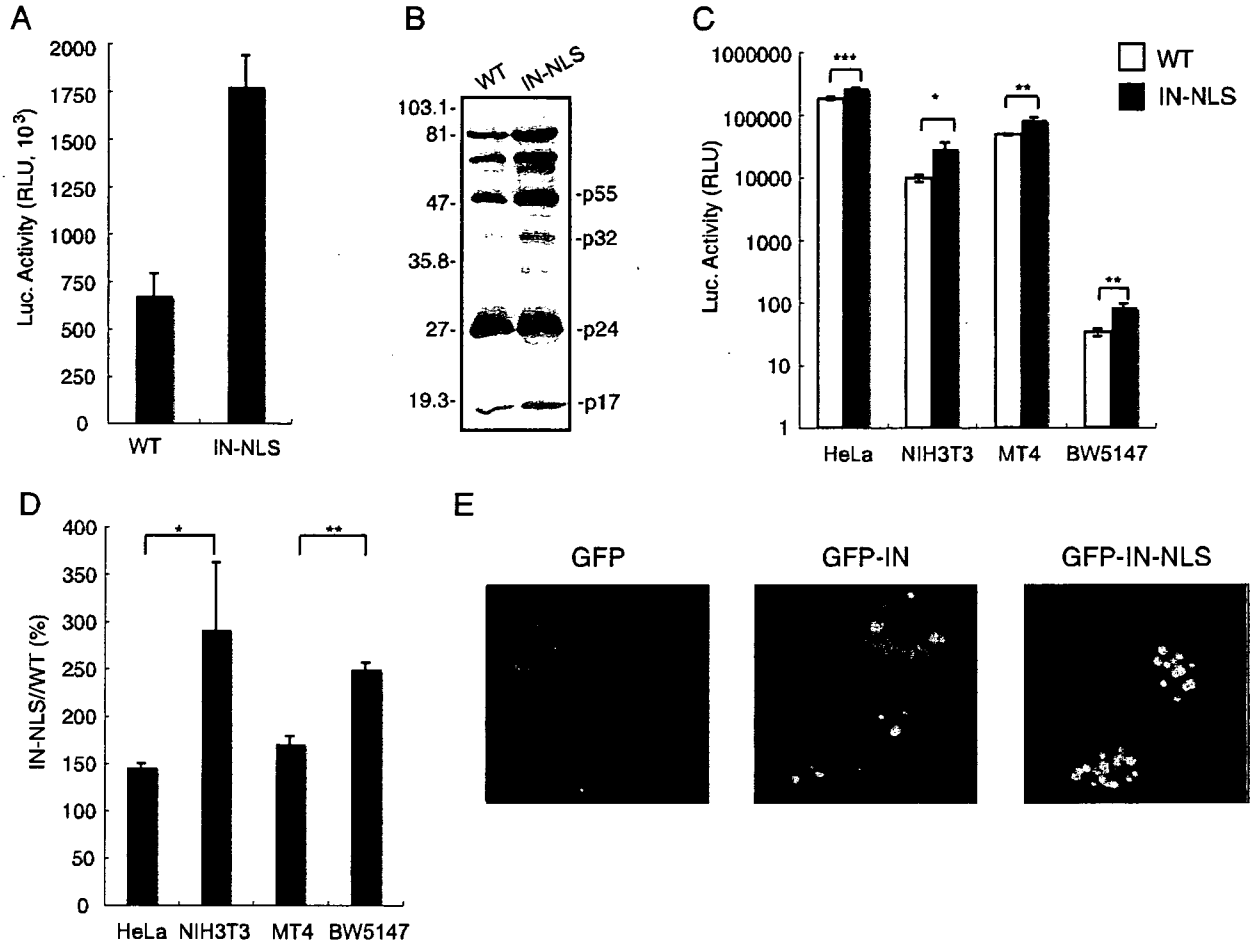

FIG. 8. Enhancement of viral infectivity to mouse cells by the addition of SV40 NLS to the C terminus of IN. (A) Luciferase activity in an HIV-1 pNL43lucΔenv vector (WT) or pNL43lucΔenv vector carrying an SV40 NLS-ligated IN (IN-NLS)-transfected 293T cells were measured at 2 days posttransfection. The data were reproduced in 10 independent experiments. (B) Virus particles were collected at 48 h posttransfection and resuspended in PBS. The viral pellets were hearted at 90°C for 10 min in the presence of sample buffer (62.5 mM Tris-HCl, pH 6.8, 10% glycerol, 2% SDS, 5% 2-mercaptoethanol, 0.005% bromophenol blue). Then viral proteins were electrophoresed on a 12% SDS–polyacrylamide gel. Viral proteins were detected with AIDS patient serum. Positions of the major viral proteins are indicated together with molecular weight markers. (C) Human and mouse cells were infected with equivalent amounts of WT (□) or IN-NLS (■) virus at 37°C for 6 h, and then the virus was removed. The luciferase activity was measured 4 days after infection, and the activity was normalized relative to the total amount of protein. Means ± SEM are shown. (D) Relative Luc activities of IN-NLS virus-infected cells compared to WT virus-infected cells were calculated using the data shown in panel C. Means ± SEM are shown. (E) NIH 3T3 cells transfected with a plasmid expressing GFP, GFP-IN, or GFP-IN-NLS fusion protein were analyzed by confocal microscopy. At 24 h posttransfection, cells were fixed and GFP was detected by a confocal fluorescent microscope. *, $P < 0.05$; **, $P < 0.01$; ***, $P < 0.001$ (by Student's t test).

SV40 NLS to the C terminus of IN significantly enhanced viral infectivity in all cell lines used (Fig. 8C). As the NLS fusion at the C terminus of IN disrupted the *vif* gene, we did not analyze the infectivity to human PBMC, which was nonpermissive to *vif*-deficient virus (24, 69). Interestingly, the effect of the NLS on viral infection was significantly stronger in mouse cells than in human cells (Fig. 8D).

We also analyzed the karyophilic property of GFP-IN-NLS in which EGFP was fused to the N terminus and the SV40 NLS at the C terminus of IN. GFP-IN-NLS accumulated almost exclusively in the nucleus of NIH 3T3 cells, in contrast to GFP-IN (Fig. 8E). These results indicate that the addition of functional NLS to IN compensates the functional defects of IN in mouse cells.

DISCUSSION

HIV-1 replication in rodent cells is blocked at multiple steps, including viral entry, transcription, nuclear export of the mRNA, assembly, and budding (77). In this study, we demonstrated that an additional host range barrier is present in mouse cells at the PIC nuclear transport step. We suggest that this restriction is caused by the dysfunction of the HIV-1 IN-dependent PIC import system.

We found that the ratio of the 2-LTR circular product to the late reverse transcription product (R-gag), which are produced in the nucleus and cytoplasm, respectively, was decreased in mouse splenocytes relative to human PBMCs after infection with both HIV-1/MuLV and HIV-1/VSV-G pseudotyped vi-

ruses (Fig. 6, lower panels). This indicates a reduction in nuclear import of the PIC. The efficiency of nuclear transfer of the viral PIC was recently reported to be reduced in mouse T cells relative to human T cell lines, but not in NIH 3T3 cells (7). These results are consistent with ours, although we cannot explain their lack of reduction in the NIH 3T3 cells. Our system using the IN mutant virus is probably more sensitive in detecting the defect.

We showed that the infection efficiency, as determined by luciferase activity, was 10 to 100, 100 to 1,000, and >1.000 times lower than in human cells in mouse adherent cells, T cell lines, and primary cells, respectively (Fig. 4). As the PIC nuclear import reduction in mouse cells was at most 60 to 90% compared to human cells (Fig. 6), it is clear that other barriers are also involved in the HIV-1 replication restriction in mouse cells. In this regard, we showed that the 2-LTR/R-gag ratio following infection with WT HIV-1 was similar between HeLa and NIH 3T3 cells and between MT4 and BW5147 cells, in contrast to our observations with the IN-deficient mutant virus (Fig. 6, lower panels). These results are explainable if the R-gag products integrate rapidly into the host chromosome in human cells compared to mouse cells, assuming that a constant proportion of free R-gag products is converted into the 2-LTR form. Thus, integration of the R-gag products into the host chromosome may also be inhibited in mouse cells. In accordance with this idea, we demonstrated that the integration frequency of HIV-1 was greatly reduced upon infection with WT HIV-1 in mouse cells transgenic for the huCD4/CXCR4 genes.

There are two formal explanations for the inability of the mouse cells to support HIV-1 PIC nuclear import. One is the absence of a required human-specific factor, and the other is the presence of an inhibitory factor(s) in mouse cells. However, because mouse-human cell fusions allow viral replication, mouse cells most likely do not have such an inhibitory factor and are rather devoid of a critical factor for the import of the HIV-1 PIC (52).

Although the mechanisms of PIC nuclear import have not been elucidated completely, NLSs are present in three viral proteins (MA, Vpr, and IN) as well as in a central DNA flap produced during reverse transcription that also contributes to the successful nuclear targeting of the PIC (59, 64, 71). Although their respective contributions remain controversial and unclear, it has been clearly shown that both Vpr and IN are karyophilic and rapidly accumulate in the nuclei of infected cells (6, 16, 19, 20, 25, 32, 48, 63, 66, 68). Meanwhile, localization of MA to the nucleus is not well established (14, 23). In this report, we demonstrated that GFP-fused IN remained in the cytoplasm of NIH 3T3 cells, in contrast to its accumulation in the nuclei of HeLa cells. On the other hand, when GFP-fused Vprs were examined, they localized to the nuclei of both NIH 3T3 and HeLa cells. The nuclear distribution of GFP-IN, but not GFP-fused Vpr, was also inhibited in the Colon-26 mouse cell line. These observations indicate that Vpr can be imported into the nucleus using separate pathways. IN, on the other hand, cannot be imported efficiently into the nuclei of mouse cells, and this is probably due to the inability of IN to interact with mouse nuclear import system.

In support for this notion, we showed that nuclear import of IN was much more enhanced in mouse cells than in human cells when authentic SV40 NLS was added to IN (Fig. 8). Furthermore, the addition of this NLS to IN significantly enhanced the infectivity of HIV-1 pseudovirus to mouse cells. These results indicate that endogenous nuclear localization signals of IN are not fully functional in mouse cells.

In this context, it is known that the NLSs within HIV-1 IN are composed of basic amino acid-rich sequences that interact with importin β through the adapter importin (25). We previously showed, however, that mutational disruption of the suggested NLSs could not abolish the nuclear localization of a GFP-IN fusion protein (76). Recent studies have shown that nonclassical NLSs are necessary and sufficient to locate the viral PIC into the nuclei (12). Depienne et al. suggested that the in vitro nuclear import of IN does not require known cytosolic transport factors, including karyopherin β family proteins (18). Two proteins have recently been reported to mediate PIC import. The first is lens epithelium-derived growth factor (LEDGF/p75), a protein implicated in the regulation of gene expression and cellular stress responses. LEDGF interacts with HIV-1 IN in vitro and in living cells (50) and colocalizes with HIV-IN in the nuclei of human cells (15). The second is importin 7, a mildly hydrophobic protein belonging to the importin β superfamily. This protein is suggested to interact with basic proteins, such as IN, that bind viral nucleic acids (21). It is currently unclear which protein(s) is important in these processes and defective in mouse cells. Clearly, further work is necessary to identify the host cell factors that are associated with IN in human cells and defective in mouse cells.

Thus far, several host restriction factors are known to be involved in the suppression of HIV-1 replication in the early phase of its life cycle in mouse cells. Friend virus susceptibility factor-1 (Fv-1) is involved in the restriction of specific mouse cell genotypes to MuLV (10, 28). The Fv-1 targets the MuLV capsid and stops the nuclear import of the PIC (8, 39). However, recent reports have noted that there is no correlation between HIV-1 susceptibility and cellular Fv-1 genotype (7, 31). Tripartite motif 5 α (TRIM5α), encoded by the gene *Lv-1*, is another restriction factor (72). TRIM5α inhibits viral replication in rhesus macaque cells at a step after entry but before the reverse transcription of HIV-1 by targeting the viral capsid protein (60). Thus, both Fv-1 and TRIM5α function in processes other than the transport of PIC into the nucleus.

In conclusion, we have demonstrated that PIC nuclear import is blocked in mouse cells and that dysfunctional IN is at least partially responsible for the barrier. Further characterization and identification of factors that are involved in PIC nuclear import should provide new insight into the molecular mechanisms of the PIC import step and clues to the development of new therapeutics. Furthermore, identification of the factors responsible for this step will assist in our generation of transgenic small animal models that are permissive to HIV-1 infection.

ACKNOWLEDGMENTS

We thank Takao Masuda (Tokyo Dental and Medical University) for providing pNL43lucΔenv and an amphotropic Moloney MuLV envelope expression vector (pJD-1) as well as for critical discussions. We also thank Yoshio Koyanagi (Kyoto University) for providing the 2-LTR plasmid and the AIDS patient serum and for important technical advice. We also thank Yoshio Inagaki (Tokyo Medical and Dental University) for providing the AIDS patient serum. We are grateful

to Luigi Naldini (San Raffaele Telethon Institute for Gene Therapy) and Kenzaburo Tani (Kyushu University) for providing the VSV-G envelope-expressing plasmid (pMD-G).

This work was supported by Grants-in-Aid from the Japan Human Sciences Foundation.

REFERENCES

1. **Adachi, A., H. E. Gendelman, S. Koenig, T. Folks, R. Willey, A. Rabson, and M. A. Martin.** 1986. Production of acquired immunodeficiency syndrome-associated retrovirus in human and nonhuman cells transfected with an infectious molecular clone. J. Virol. 59:284–291.
2. **Aiken, C.** 1997. Pseudotyping human immunodeficiency virus type 1 (HIV-1) by the glycoprotein of vesicular stomatitis virus targets HIV-1 entry to an endocytic pathway and suppresses both the requirement for Nef and the sensitivity to cyclosporin A. J. Virol. 71:5871–5877.
3. **Alonso, A., T. P. Cujec, and B. M. Peterlin.** 1994. Effects of human chromosome 12 on interactions between Tat and TAR of human immunodeficiency virus type 1. J. Virol. 68:6505–6513.
4. **Alonso, A., D. Derse, and B. M. Peterlin.** 1992. Human chromosome 12 is required for optimal interactions between Tat and TAR of human immunodeficiency virus type 1 in rodent cells. J. Virol. 66:4617–4621.
5. **Bai, Y., Y. Soda, K. Izawa, T. Tanabe, X. Kang, A. Tojo, H. Hoshino, H. Miyoshi, S. Asano, and K. Tani.** 2003. Effective transduction and stable transgene expression in human blood cells by a third-generation lentiviral vector. Gene Ther. 10:1446–1457.
6. **Balliet, J. W., D. L. Kolson, G. Eiger, F. M. Kim, K. A. McGann, A. Srinivasan, and R. Collman.** 1994. Distinct effects in primary macrophages and lymphocytes of the human immunodeficiency virus type 1 accessory genes vpr, vpu, and nef: mutational analysis of a primary HIV-1 isolate. Virology 200:623–631.
7. **Baumann, J. G., D. Unutmaz, M. D. Miller, S. K. Breun, S. M. Grill, J. Mirro, D. R. Littman, A. Rein, and V. N. KewalRamani.** 2004. Murine T cells potently restrict human immunodeficiency virus infection. J. Virol. 78:12537–12547.
8. **Benit, L., N. De Parseval, J. F. Casella, I. Callebaut, A. Cordonnier, and T. Heidmann.** 1997. Cloning of a new murine endogenous retrovirus, MuERV-L, with strong similarity to the human HERV-L element and with a gag coding sequence closely related to the Fv1 restriction gene. J. Virol. 71:5652–5657.
9. **Berson, J. F., D. Long, B. J. Doranz, J. Rucker, F. R. Jirik, and R. W. Doms.** 1996. A seven-transmembrane domain receptor involved in fusion and entry of T-cell-tropic human immunodeficiency virus type 1 strains. J. Virol. 70:6288–6295.
10. **Best, S., P. Le Tissier, G. Towers, and J. P. Stoye.** 1996. Positional cloning of the mouse retrovirus restriction gene Fv1. Nature 382:826–829.
11. **Bieniasz, P. D., and B. R. Cullen.** 2000. Multiple blocks to human immunodeficiency virus type 1 replication in rodent cells. J. Virol. 74:9868–9877.
12. **Bouyac-Bertoia, M., J. D. Dvorin, R. A. Fouchier, Y. Jenkins, B. E. Meyer, L. I. Wu, M. Emerman, and M. H. Malim.** 2001. HIV-1 infection requires a functional integrase NLS. Mol. Cell 7:1025–1035.
13. **Browning, J., J. W. Horner, M. Pettoello-Mantovani, C. Raker, S. Yurasov, R. A. DePinho, and H. Goldstein.** 1997. Mice transgenic for human CD4 and CCR5 are susceptible to HIV infection. Proc. Natl. Acad. Sci. USA 94:14637–14641.
14. **Bukrinsky, M., K. Manogue, and A. Cerami.** 1995. HIV results in the frame. Other approaches. Nature 375:195–196. (Author's reply, 375:198.)
15. **Cherepanov, P., G. Maertens, P. Proost, B. Devreese, J. Van Beeumen, Y. Engelborghs, E. De Clercq, and Z. Debyser.** 2003. HIV-1 integrase forms stable tetramers and associates with LEDGF/p75 protein in human cells. J. Biol. Chem. 278:372–381.
16. **Connor, R. I., B. K. Chen, S. Choe, and N. R. Landau.** 1995. Vpr is required for efficient replication of human immunodeficiency virus type-1 in mononuclear phagocytes. Virology 206:935–944.
17. **Cullen, B. R.** 2001. Journey to the center of the cell. Cell 105:697–700.
18. **Depienne, C., A. Mousnier, H. Leh, E. Le Rouzic, D. Dormont, S. Benichou, and C. Dargemont.** 2001. Characterization of the nuclear import pathway for HIV-1 integrase. J. Biol. Chem. 276:18102–18107.
19. **Depienne, C., P. Roques, C. Creminon, L. Fritsch, R. Casseron, D. Dormont, C. Dargemont, and S. Benichou.** 2000. Cellular distribution and karyophilic properties of matrix, integrase, and Vpr proteins from the human and simian immunodeficiency viruses. Exp. Cell Res. 260:387–395.
20. **Farnet, C. M., B. Wang, J. R. Lipford, and F. D. Bushman.** 1996. Differential inhibition of HIV-1 preintegration complexes and purified integrase protein by small molecules. Proc. Natl. Acad. Sci. USA 93:9742–9747.
21. **Fassati, A., D. Gorlich, I. Harrison, L. Zaytseva, and J. M. Mingot.** 2003. Nuclear import of HIV-1 intracellular reverse transcription complexes is mediated by importin 7. EMBO J. 22:3675–3685.
22. **Feng, Y., C. C. Broder, P. E. Kennedy, and E. A. Berger.** 1996. HIV-1 entry cofactor: functional cDNA cloning of a seven-transmembrane, G protein-coupled receptor. Science 272:872–877.
23. **Fouchier, R. A., B. E. Meyer, J. H. Simon, U. Fischer, and M. H. Malim.** 1997. HIV-1 infection of non-dividing cells: evidence that the amino-terminal basic region of the viral matrix protein is important for Gag processing but not for post-entry nuclear import. EMBO J. 16:4531–4539.
24. **Gabuzda, D. H., H. Li, K. Lawrence, B. S. Vasir, K. Crawford, and E. Langhoff.** 1994. Essential role of vif in establishing productive HIV-1 infection in peripheral blood T lymphocytes and monocyte/macrophages. J. Acquir. Immune Defic. Syndr. 7:908–915.
25. **Gallay, P., T. Hope, D. Chin, and D. Trono.** 1997. HIV-1 infection of nondividing cells through the recognition of integrase by the importin/karyopherin pathway. Proc. Natl. Acad. Sci. USA 94:9825–9830.
26. **Garber, M. E., and K. A. Jones.** 1999. HIV-1 Tat: coping with negative elongation factors. Curr. Opin. Immunol. 11:460–465.
27. **Garber, M. E., P. Wei, V. N. KewalRamani, T. P. Mayall, C. H. Herrmann, A. P. Rice, D. R. Littman, and K. A. Jones.** 1998. The interaction between HIV-1 Tat and human cyclin T1 requires zinc and a critical cysteine residue that is not conserved in the murine CycT1 protein. Genes Dev. 12:3512–3527.
28. **Goff, S. P.** 1996. Operating under a Gag order: a block against incoming virus by the Fv1 gene. Cell 86:691–693.
29. **Habu, K., J. Nakayama-Yamada, M. Asano, S. Saijo, K. Itagaki, R. Horai, H. Yamamoto, T. Sekiguchi, T. Nosaka, M. Hatanaka, and Y. Iwakura.** 1999. The human T cell leukemia virus type I-tax gene is responsible for the development of both inflammatory polyarthropathy resembling rheumatoid arthritis and noninflammatory ankylotic arthropathy in transgenic mice. J. Immunol. 162:2956–2963.
30. **Hart, C. E., C. Y. Ou, J. C. Galphin, J. Moore, L. T. Bacheler, J. J. Wasmuth, S. R. Petteway, Jr., and G. Schochetman.** 1989. Human chromosome 12 is required for elevated HIV-1 expression in human-hamster hybrid cells. Science 246:488–491.
31. **Hatziioannou, T., S. Cowan, and P. D. Bieniasz.** 2004. Capsid-dependent and -independent postentry restriction of primate lentivirus tropism in rodent cells. J. Virol. 78:1006–1011.
32. **Heinzinger, N. K., M. I. Bukinsky, S. A. Haggerty, A. M. Ragland, V. Kewalramani, M. A. Lee, H. E. Gendelman, L. Ratner, M. Stevenson, and M. Emerman.** 1994. The Vpr protein of human immunodeficiency virus type 1 influences nuclear localization of viral nucleic acids in nondividing host cells. Proc. Natl. Acad. Sci. USA 91:7311–7315.
33. **Ho, S. N., H. D. Hunt, R. M. Horton, J. K. Pullen, and L. R. Pease.** 1989. Site-directed mutagenesis by overlap extension using the polymerase chain reaction. Gene 77:51–59.
34. **Hogan, B., E. Constantini, and E. Lacey.** 1994. Manipulating the mouse embryo: a laboratory manual, 2nd ed. Cold Spring Harbor Laboratory Press, Cold Spring Harbor, NY.
35. **Isegawa, Y., J. Sheng, Y. Sakawa, K. Yamanishi, O. Nakagomi, and S. Ueda.** 1992. Selective amplification of cDNA sequence from total RNA by cassette-ligation mediated polymerase chain reaction (PCR): application to sequencing 6.5 kb genome segment of hantavirus strain B-1. Mol. Cell Probes 6:467–475.
36. **Iwakura, Y., T. Shioda, M. Tosu, E. Yoshida, M. Hayashi, T. Nagata, and H. Shibuta.** 1992. The induction of cataracts by HIV-1 in transgenic mice. AIDS 6:1069–1075.
37. **Jackson, J. B., K. L. MacDonald, J. Cadwell, C. Sullivan, W. E. Kline, M. Hanson, K. J. Sannerud, S. L. Stramer, N. J. Fildes, S. Y. Kwok, et al.** 1990. Absence of HIV infection in blood donors with indeterminate western blot tests for antibody to HIV-1. N. Engl. J. Med. 322:217–222.
38. **Jolicoeur, P., and D. Baltimore.** 1976. Effect of Fv-1 gene product on proviral DNA formation and integration in cells infected with murine leukemia viruses. Proc. Natl. Acad. Sci. USA 73:2236–2240.
39. **Jolicoeur, P., and E. Rassart.** 1980. Effect of Fv-1 gene product on synthesis of linear and supercoiled viral DNA in cells infected with murine leukemia virus. J. Virol. 33:183–195.
40. **Keppler, O. T., W. Yonemoto, F. J. Welte, K. S. Patton, D. Iacovides, R. E. Atchison, T. Ngo, D. L. Hirschberg, R. F. Speck, and M. A. Goldsmith.** 2001. Susceptibility of rat-derived cells to replication by human immunodeficiency virus type 1. J. Virol. 75:8063–8073.
41. **Klatzmann, D., E. Champagne, S. Chamaret, J. Gruest, D. Guetard, T. Hercend, J. C. Gluckman, and L. Montagnier.** 1984. T-lymphocyte T4 molecule behaves as the receptor for human retrovirus LAV. Nature 312:767–768.
42. **Koito, A., Y. Kameyama, C. Cheng-Mayer, and S. Matsushita.** 2003. Susceptibility of mink (Mustera vision)-derived cells to replication by human immunodeficiency virus type 1. J. Virol. 77:5109–5117.
43. **Koito, A., H. Shigekane, and S. Matsushita.** 2003. Ability of small animal cells to support the postintegration phase of human immunodeficiency virus type-1 replication. Virology 305:181–191.
44. **Kukolj, G., K. S. Jones, and A. M. Skalka.** 1997. Subcellular localization of avian sarcoma virus and human immunodeficiency virus type 1 integrases. J. Virol. 71:843–847.
45. **Kwok, S., D. E. Kellogg, N. McKinney, D. Spasic, L. Goda, C. Levenson, and J. J. Sninsky.** 1990. Effects of primer-template mismatches on the polymerase chain reaction: human immunodeficiency virus type 1 model studies. Nucleic Acids Res. 18:999–1005.